

Dārta Ūbele-Kalniņa

**THE INFLUENCE OF CALCIUM PHOSPHATE
STRUCTURE ON THE SURFACE CHARGE
PRODUCED IN AN ELECTRIC FIELD**

Summary of the Doctoral Thesis

RIGA TECHNICAL UNIVERSITY
Faculty of Materials Science and Applied Chemistry
Institute of Materials and Surface Engineering

Dārta Ūbele-Kalniņa

Doctoral Student of the Study Programme “Materials Science”

**THE INFLUENCE OF CALCIUM PHOSPHATE
STRUCTURE ON THE SURFACE CHARGE
PRODUCED IN AN ELECTRIC FIELD**

Summary of the Doctoral Thesis

Scientific supervisor
Professor Dr. sc. ing.
KĀRLIS AGRIS GROSS

RTU Press
Riga 2023

Ūbele-Kalniņa, D. The Influence of Calcium Phosphate Structure on the Surface Charge Produced in an Electric Field. Summary of the Doctoral Thesis. Riga: RTU Press, 2023. – 43 p.

Published in accordance with the decision of the Promotion Council “RTU P-02” of 24 May 2023, Minutes No. 04030-9.2.2/4.

This work has been supported by the European Social Fund within the Project No. 8.2.2.0/20/I/008 “Strengthening of PhD students and academic personnel of Riga Technical University and BA School of Business and Finance in the strategic fields of specialization” of the Specific Objective 8.2.2 “To Strengthen Academic Staff of Higher Education Institutions in Strategic Specialization Areas” of the Operational Programme “Growth and Employment”



NACIONĀLAIS
ATTĪSTĪBAS
PLĀNS 2020



EIROPAS SAVIENĪBA
Eiropas Sociālais
fonds

IEGULDĪJUMS TAVĀ NĀKOTNĒ

This research was supported by Riga Technical University Doctoral Grant programme, Latvian Council of Science project No. 2018/01-0432 “Freedom to Move – Directing stored energy from metastable materials for improving implant properties” and M-Era.net project No. ESRTD/2017/4 “Implants signal to bone for bone growth and attachment”.

<https://doi.org/10.7250/9789934229473>
ISBN 978-9934-22-947-3 (pdf)

DOCTORAL THESIS PROPOSED TO RIGA TECHNICAL UNIVERSITY FOR THE PROMOTION TO THE SCIENTIFIC DEGREE OF DOCTOR OF SCIENCE

To be granted the scientific degree of Doctor of Science (Ph. D.), the present Doctoral Thesis has been submitted for the defence at the open meeting of RTU Promotion Council on September 8, 2023 at 12:00 online on Zoom:

<https://rtucloud1.zoom.us/j/98800814512?pwd=SXloZ0hxV29HTGF5TWdMQVVKOFZQU T09>.

OFFICIAL REVIEWERS

Professor Dr. sc. ing. Jānis Ločs,
Riga Technical University

Dr. phys. Anatolijs Popovs,
Institute of Solid State Physics, University of Latvia, Latvia

Assist. Professor PhD Inga Grigoraviciute-Puroniene,
Vilnius University, Lithuania

DECLARATION OF ACADEMIC INTEGRITY

I hereby declare that the Doctoral Thesis submitted for the review to Riga Technical University for the promotion to the scientific degree of Doctor of Science (Ph. D.) is my own. I confirm that this Doctoral Thesis had not been submitted to any other university for the promotion to a scientific degree.

Dārta Ūbele-Kalniņa (signature)

Date:

The Doctoral Thesis has been written in Latvian. It consists of an Introduction, 3 chapters, Conclusions, 58 figures, 13 tables, 10 appendices; the total number of pages is 128, including appendices. The Bibliography contains 210 titles.

ACKNOWLEDGEMENTS

I would like to thank my supervisor Professor Kārlis Agris Gross for the opportunity to conduct research in the field of calcium phosphate biomaterials and the opportunity to participate in scientific projects during my doctoral studies.

I am grateful to the leading researchers of the Faculty of Chemistry of the University of Latvia, Professor Arturs Vīksna for providing access to the FTIR spectrometer and providing ICP-MS and ICP-OES measurements; Dr. chem. Agris Bērziņš for access to XRD measurements.

Many thanks to the leading researcher of the National Science Platform FOTONIKA-LV of the University of Latvia, Dr. phys. Arnolds Ūbelis for his support in the preparation of vacuum-heated samples and help in editing the PhD Thesis. Thanks to glassblower Aleksandr Kapralov for creating quartz ampoules for research in vacuum.

Huge thanks to the colleagues from the Faculty of Materials Science and Applied Chemistry for providing assistance and access to research facilities. Special thanks to Astrīda Bērziņa for her help with AFM measurements, Raman measurements and discussions during the PhD studies. Thanks to the guys from the Institute of Technical Physics for providing the picoammeter in the initial research and advising on the improvement of the surface charge measurement system. Thanks to Ints Šteins for producing SPS pellets. Thanks to my colleagues from the former Biomaterials Research Laboratory, especially Dr. sc. ing. Liene Plūduma (*Liene Pluduma-LaFarge*) for her help in the first years of my PhD studies; Aiga Anna Jokša for the pressed pellets and help in developing articles; Ilze Jerāne for measurements on coatings.

I am grateful to my family and friends for their immense support, inspiring and encouraging me throughout my PhD studies.

CONTENTS

ACKNOWLEDGEMENTS	4
ABBREVIATIONS AND TERMS.....	6
INTRODUCTION.....	7
Aim of the Doctoral Thesis	8
Tasks of the Doctoral Thesis	8
Thesis statements to be defended	8
Scientific novelty.....	9
Practical significance.....	9
Approbation of the research	9
1. LITERATURE REVIEW.....	11
2. METHODS.....	13
3. RESULTS AND DISCUSSION	16
3.1. Characterization of thermally sprayed hydroxyapatite droplets	16
3.2. Determination of OH ⁻ ions in calcium phosphates	19
3.2.1. Incorporation of OH ⁻ ions into the HAp coating structure	19
3.2.2. Characterization of OH ⁻ ions in the amorphous phase using a new technique	22
3.3. Measurement of surface charges	27
3.3.1. Inter-laboratory study of electrical polarization and TSDC measurements	27
3.3.2. Surface charge measurements on SPS pellets	30
3.3.3. Effect of polarization temperature on the magnitude of the surface charge	34
3.3.4. Surface charge of apatite coatings of different structures	36
3.3.5. Effect of surface charge on the contact angle of apatite coatings of different structures	37
CONCLUSIONS	38
References	39

ABBREVIATIONS AND TERMS

ACP	amorphous calcium phosphate
α -TCP	alpha tricalcium phosphate
β -TCP	beta tricalcium phosphate
cACP	carbonate-containing amorphous calcium phosphate
CaP	calcium phosphate
Ca/P	molar ratio of calcium and phosphorus
CHAp	carbonate-containing hydroxyapatites
DC	direct current
E_a	activation energy
E_p	the electric field used in electric polarization
FTIR	Fourier transform infrared spectroscopy
HAp	hydroxyapatite, $\text{Ca}_{10}(\text{PO}_4)_6(\text{OH})_2$.
HT	hydrothermal
ICDD	International Centre for Diffraction Data
ICP-MS	inductively coupled plasma mass spectrometry
ICP-OES	inductively coupled plasma optical emission spectrometry
<i>In vitro</i>	process performed in a test tube or elsewhere outside a living organism
<i>In vivo</i>	process carried out or taking place in a living organism
OAp	oxyapatite
pA	pico ampere
SEM	scanning electron microscopy
SPS	spark plasma sintering
T_p	polarization temperature
t_p	polarization time at T_p
TTCP	tetracalcium phosphate
TSDC	thermally stimulated depolarization currents
Q	charge density
XRD	X-ray diffractometry

INTRODUCTION

It is generally known that research and new knowledge, which create opportunities to purposefully create bioceramics with the necessary properties, are vital for improving the quality of society's life. Orthopaedic bioceramic materials play a key role in bone regeneration. However, problems remain with bone implants, and risks of infection compromise recovery from surgery and the ability of the implant to function [1], [2]. Therefore, it is necessary to further study and improve properties of the bone implants.

Hydroxyapatite (HAp) is an inorganic calcium phosphate that is chemically and structurally similar to the mineral in bones and teeth: non-stoichiometric in chemistry with many elemental substitutions in the structure [3]. Therefore, synthesized HAp provides a good structural and chemical basis for improved biocompatibility of orthopaedic implants and better bone tissue attachment.

Various electrical signals participate in ensuring the life processes of living organisms, for example, to receive and transmit muscle contractions or nerve impulses. Vertebrate bones, on the other hand, possess the ability to generate electrical potential [4, [5], which is essential for bone regeneration [5], [6]. Studies have shown that an electrical potential is formed at the bone fracture site that assists the bone healing process [5], [7]. It is possible to artificially imitate and study these processes found in nature, while the acquired knowledge can be purposefully used to improve natural processes. While studying the natural processes in bone regeneration, the possibility of artificially created additional electric charges has been found. For bone implants created in this way with additional surface charges, it is possible to create a particularly favourable environment for bone cells to improve the faster absorption of the implant material into the body.

Hydroxyapatite can be polarized to an electret by applying an electric field at an elevated temperature [8]. Surface charge generated by electrical polarization results in novel material properties that promote bone cell formation on electrically charged HAp ceramic surfaces both *in vitro* [9]–[11] and *in vivo* [12]–[14]. Such improvements provide opportunities to diversify the properties of bone biomaterials in order to optimize bone healing processes and reduce the time of implant integration.

Previous publications have reported on only several polarized calcium phosphates: hydroxyapatite, carbonated apatite and several chemically substituted hydroxyapatites. There has been no mention of textured apatites, amorphous calcium phosphate, and the effect of hydroxyl content on creating a surface charge. Amorphous calcium phosphate (ACP), with a lower hardness and higher solubility that crystallizes to hydroxyapatite at lower temperatures could secure a higher surface electric charge compared to a crystalline material conventionally heated at high temperatures.

Calcium phosphates have lower mechanical properties than natural hard tissues that contain an organic phase (collagen) for improved mechanical properties. It is possible to improve mechanical properties of calcium phosphates in a coating form on biocompatible metals. This study uses the thermal spray method for forming individual droplets and coatings with different structures. Methods for optimizing thermally sprayed coatings will be addressed –

incorporation of OH⁻ ions (OH⁻) into the HAp structure, and production of surface charge by polarization in an electric field.

Very few studies have been published on polarized apatites. Equipment for polarization and current measurement are tailor made in laboratories and not commercially available. There is no calibration standard, therefore the first step is to produce this equipment and conduct an inter-laboratory study to show the validity of the method. This will support the production and show the trustworthiness of measured surface charges for the next generation implants. The research direction of this Doctoral Thesis involves surface charges created in an electric field and quantification of charge on different calcium phosphates. In the course of the work, various calcium phosphates have been produced – as coatings and pellets – and then characterized.

Aim of the Doctoral Thesis

Produce calcium phosphates with different structures and determine whether they can be electrically charged. Quantify surface charge and determine the properties of materials with and without a surface charge.

Tasks of the Doctoral Thesis

1. Create apatites as pellets and coatings in different phases (amorphous, crystalline with oriented and randomly oriented crystals) and then characterize the apatites by appropriate analytical methods.
2. Determine the OH⁻ content in thermally sprayed coatings and the best conditions for incorporating OH⁻ into the structure.
3. Test for the ability to detect OH⁻ in amorphous calcium phosphates after vacuum heating.
4. Electrically polarize calcium phosphate and quantify surface charge to:
 - a. determine the repeatability of electric charge quantification in an inter-laboratory study;
 - b. investigate the ability to impart and then measure the surface charge on amorphous calcium phosphate made by wet-precipitation or thermal-spraying;
 - c. study the effect of polarization temperature on surface charge for thermally sprayed HAp with an oriented crystal structure;
 - d. compare the electric charge on calcium phosphates with different crystal structures.
5. Determine the effect of surface charge on the wettability of calcium phosphate coatings.

Thesis statements to be defended

1. A surface charge can be imparted on amorphous calcium phosphate by electric polarization by ordering the initially disordered structure in an electric field.
2. The stored surface charge of calcium phosphate samples is affected by both the crystalline structure and crystal orientation of these materials.

3. It is possible to obtain a crystalline phase by crystallization of amorphous calcium phosphate in vacuum and therefore estimate the OH^- ion content that was present in the initial amorphous phase.

Scientific novelty

Surface electric charges have been created and compared between calcium phosphates with different crystal structures. For the first time surface charges were created and determined on:

- amorphous calcium phosphates,
- HAp with oriented crystal structure,
- the effect of OH^- on the size of the surface charge is discussed.

A set of laboratory equipment has been created for polarizing samples in an electric field by heating them to 450 °C and determining the surface electric charge by the TSDC method (heating to 700 °C). The possibility of determining OH^- in the thermally sprayed amorphous calcium phosphate phase was established.

Practical significance

Electrical polarization and thermally stimulated depolarization current (TSDC) measurement equipment and a methodology were developed for calcium phosphate research on electrically charged surfaces and to determine surface charges at elevated temperatures.

Amorphous calcium phosphate could be electrically polarized, as shown for the first time, and the surface charges were measured using the thermally stimulated depolarization current (TSDC) method.

The surface charge and surface energy were determined on different thermally sprayed calcium phosphate coatings that showed the influence of microstructure on the electric polarization.

Approbation of the research

The scientific achievements and main results of the Doctoral Thesis have been reported at 9 international scientific conferences, published in 2 full-text scientific publications and 3 peer-reviewed publications in scientific conference proceedings.

Scientific publications:

1. Joksa, A. A., Komarovska, L., **Ubele-Kalnina, D.**, Viksna, A., Gross, K. A. Role of carbonate on the crystallization and processing of amorphous calcium phosphates, *Materialia*. 27 (2023) 101672. doi.org/10.1016/j.mtla.2022.101672. (Scopus)
2. **Ubele-Kalnina, D.**, Nakamura, M., Gross, K. A. Inter-Laboratory Study on Measuring the Surface Charge of Electrically Polarized Hydroxyapatite, *J. Funct. Biomater.* 14 (2023) 100. https://doi.org/10.3390/jfb14020100. (Scopus)

Peer-reviewed publications in scientific conference proceedings:

1. Pudule, A., Gross, K. A., **Ubele, D.**, Jerane, I., Steins, I. Densification of Amorphous Calcium Phosphate: A Comparison of Cold Sintering Processes. *Key Engineering Materials*, Vol. 903, pp. 46–51, 2021. ISBN 978-9934-22-530-7. (Scopus)
2. **Ubele, D.**, Plūduma, L., Gross, K. A., Viksna, A. Hydrothermal Processing for Increasing the Hydroxyl Ion Concentration in Hydroxyl Depleted Hydroxyapatite. *Key Engineering Materials*, pp. 42–47, 2018, ISBN 978-3-0357-1238-4. ISSN 1013-9826. doi:10.4028/www.scientific.net/KEM.762.42. (Scopus)
3. **Ubele, D.**, Pluduma, L., Brangule, A., Berzina, A., Koivuluoto, H., Vuoristo, P., Juskenas, R., Gross, K. A. Investigations on the Tailorability of Hard Tissue Implant Surfaces by Printing. *European Cells and Materials*, 2017, Vol. 33, No. 1, pp. 33–33. ISSN 1473-2262. doi:10.22203/eCM.

Presentations at conferences:

1. **Ubele-Kalnina, D.**, Gross, K. A. Improving surface wettability on hydroxyapatite coatings by electrical polarization. 63rd International Scientific Conference of Riga Technical University, Materials Science and Applied Chemistry Section – MSAC 2022, Latvia, Riga, 21.10.2022. (oral presentation)
2. **Ubele-Kalniņa, D.**, Gross, K. A. Surface charge and wettability dependence of the structure of hydroxyapatite coatings. 32nd Symposium and Annual Meeting of the International Society for Ceramics in Medicine, Italy, Venice, 20–23.09.2022. (poster presentation)
3. **Ubele, D.**, Steins, I, Valdniece, D., Pudule, A. A., Gross, K. A. Stored Charge determination of Spark Plasma Sintered Amorphous Calcium Phosphate. 79th International Scientific Conference of the University of Latvia, Section of Analytical Chemistry, 12.02.2021. (oral presentation)
4. **Ubele, D.**, Pluduma, L., Gross, K. A. Influence of hydrothermal treatment on stored charge density of thermally sprayed hydroxyapatite. 16th European Ceramic Society Conference, Italy, Turin, 16–21.06.2019. (poster presentation)
5. **Ubele, D.**, Pluduma, L., Gross, K. A. The Influence of Microstructure on the Surface Charge of Sintered Hydroxyapatite Ceramics. 59th International Scientific Conference of Riga Technical University, Materials Science and Applied Chemistry Section – MSAC 2018, Latvia, Riga, 26.10.2018. (oral presentation)
6. **Ubele, D.**, Pluduma, L., Gross, K. A. The Effect of Hydroxyl Ion Concentration on the Degree of Polarization in Thermally Sprayed Hydroxyapatite. *ESB2018 Abstract Proceedings*, the Netherlands, Maastricht, 9–13.09.2018. (poster presentation)
7. **Ubele, D.**, Pluduma, L., Gross, K. A. Increasing Hydroxyl Ion Concentration of Thermally Sprayed Hydroxyapatite Coatings by Hydrothermal Treatment. 76th International Scientific Conference of the University of Latvia, Chemistry Section, Latvia, Riga, 09.02.2018. (oral presentation)
8. **Ubele, D.**, Pluduma, L., Gross, K. A., Viksna, A. Hydrothermal Processing for Increasing the Hydroxyl Ion Concentration in Hydroxyl Depleted Hydroxyapatite. 58th International Scientific Conference of Riga Technical University, Materials Science and Applied Chemistry Section – MSAC 2017, Latvia, Riga, 20.10.2017. (poster presentation)
9. **Ubele, D.**, Pluduma, L., Brangule, A., Berzina, A., Koivuluoto, H., Vuoristo, P., Juskenas, R., Gross, K. A. Investigations on the Tailorability of Hard Tissue Implant Surfaces by Printing. 10th Conference of the Scandinavian Society of Biomaterials, "Underlying Challenges in Biomaterials", Norway, Hafjell, 15–17.03.2017. (oral presentation)

1. LITERATURE REVIEW

The literature review of the Doctoral Thesis summarizes information about calcium phosphates with a closer look at amorphous calcium phosphates (ACP), hydroxyapatite (HAp) and biological apatites. Information has been collected on the polarization of calcium phosphate (CaP) in an electric field and the magnitudes of electric charges. The mechanisms of electrical polarization and depolarization measurement methodologies are reviewed. The structure of bone, the formation of electric potential in bones, as well as the creation of thermally sprayed coatings and post-treatment with the hydrothermal method are discussed.

Stoichiometric HAp ($\text{Ca}_{10}(\text{PO}_4)_6(\text{OH})_2$) is the main inorganic component of vertebrate bones and teeth, due to which they are widely used in production of orthopaedic implants [15], bone cements [16], coatings [17], [18], etc. However, the apatite in natural bones is not stoichiometric and is substituted by various ions, e.g. Mg^{2+} , Fe^{2+} , Na^+ , K^+ , CO_3^{2-} , HPO_4^{2-} , F^- , and Cl^- [19].

ACPs are found in many biological systems where they serve as a reservoir of calcium and phosphate ions, their general formula is described as $\text{Ca}_x\text{H}_y(\text{PO}_4)_z \cdot n\text{H}_2\text{O}$ ($n = 3 - 4.5$ and contains 10–20 % H_2O) [20], they can have a Ca/P molar ratio of 1.2–2.2. ACP can be crystallized into crystalline calcium phosphates, depending on Ca/P, they have better *in vivo* bone conductivity than HAp, good biological activity, and no cytotoxicity. A growing interest in ACPs emerged due to the possible association of these compounds with vertebrate bones – ACPs have been observed to occur during early bone formation [21], [22], suggesting that ACP is a precursor in the formation of the bone mineral phase.

Compared to natural bone, HAp has low mechanical strength, therefore, in order to implant it in load-bearing sites and improve its mechanical properties, it is necessary to form coatings [23], using biocompatible materials with good mechanical properties as substrates, such as titanium. For the production of HAp coatings, thermal spraying methods are widely used, for example, flame spraying, during which the material placed in the flame is melted and sprayed at a high speed against the surface to be coated [24], any thermally stable material with a precisely defined melting point can be coated in this way, on almost any surface. However, due to the high spraying temperature (above 3000 °C), molten HAp particles can undergo thermal decomposition into TCP, TTCP, or CaO, and the formation of the ACP phase [25], as well as dehydroxylation, leading to the release of OH^- and the formation of oxyhydroxyapatite (OHAp) [26]. To ensure the chemical composition of the HAp coating, post-treatment methods can be used, which ensure the reduction of impurity phases and the appropriate OH^- content.

Studies have shown that post-treatment of thermally sprayed HAp coatings in water vapour increases the crystallinity of the HAp and reduces the impurities of dissociated phases resulting from the thermal spraying [27]–[29]. During hydrothermal treatment, OHAp reacts with water in the vapour and OH^- enters its structure by recrystallization into HAp. Water molecules promote the transformation of the amorphous phase into the crystalline HAp and significantly increase the crystallinity of the coating [27].

The natural hard tissues of vertebrates are composite materials containing the inorganic phase – HAp nano crystals, the organic phase – collagen, and water, which ensures the strength

of the bones and adaptability to changes [19]. Bone-forming HAp crystals possess piezoelectric properties [30], resulting in the conversion of mechanical stress into electrical stimulation. This stimulus generates electrical potentials at the bone's fracture sites, which then help the bone to grow back together. Because of these observations, there has been a wide interest in applying an electric charge to the surfaces of artificially synthesized HAp implants, which can provide improved properties of biomaterials both *in vitro* [9]–[11] and *in vivo* [12]–[14].

Electrically charged HAp surfaces can be created using the method of electric polarization, i.e., by applying a DC voltage to the sample at an elevated temperature, holding it for a certain time and maintaining the electric field while cooling to room temperature. As a result, an electric surface charge is generated on the sample. Previous studies [96]–[98] have shown that increasing of the polarization temperature increases the resulting surface charge density, while there is ambiguous information on the effect of polarization time on the amount of surface charge [31], [32]. The surface charge created by the electric field on the HAp surface remains constant for at least 2 months [13].

One of the most widely used methods for determination of the electric charge on the HAp surface is the thermally stimulated depolarization current (TSDC) method, which is directly related to electrical polarization – when the temperature of an electrically polarized sample is increased, the trapped charges are gradually released, which creates a depolarization current [33]. The surface charge density can be calculated from this current.

The TSDC curves show that two mechanisms are responsible for the polarizability of HAp – dipole and space charge polarization [34]. HAp samples can have up to four polarization states (see Fig. 1.1) with different activation energies and relaxation times [32], [34].

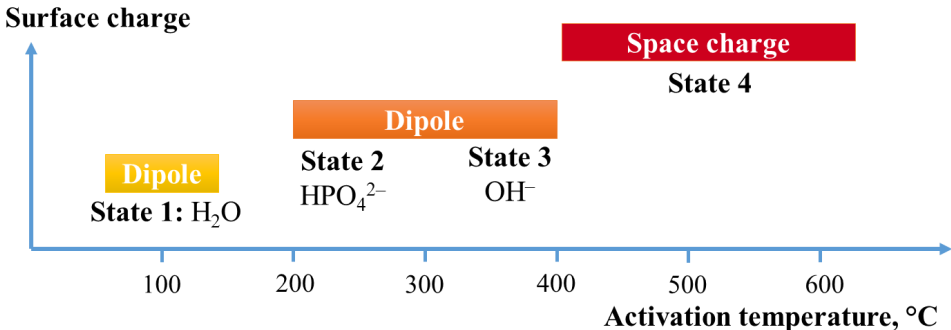


Fig. 1.1. Mechanisms of surface charge formation on the surface of Hap. (Created based on information provided in previously published studies [32], [34]).

2. METHODS

Preparation and characterization of calcium phosphate samples

HAp coatings with $\langle 001 \rangle$ crystal orientation were fabricated by the thermal spray method by flame spraying commercial HAp spray powder (particle size 25–45 μm) onto a commercially pure (Grade 1) titanium substrate (12 mm diameter, grit blasted with Al_2O_3) positioned 12 cm away from the flame and preheated to 400 °C. Part of the created coatings was used for hydrothermal (HT) treatment studies at 200 °C and 250 °C temperature and holding times of 6–48 h to determine the most optimal parameters for incorporating OH^- back into the HAp structure. Initially, a series of measurements of several individually sprayed droplets was carried out to find out the most optimal parameters for thermal spraying of HAp coatings using two substrate heating temperatures (100 °C and 400 °C) and different sputtering distances (from 4 to 20 cm).

The ACP coatings were produced by flame spraying in the same way as the HAp coatings, only in this case the substrate was cooled with liquid nitrogen and the sprayed powder was additionally cooled with carbon dioxide. Unfortunately, the thermal spraying process did not yield completely amorphous calcium phosphate coatings, but CaP coatings with low crystalline content. To obtain crystalline HAp coatings with random crystal orientation, CaP coatings with low crystalline content were HT treated at 250 °C for 12 h.

High-density HAp tablets were produced by calcination of commercial HAp powder for 2 h at 850 °C. The calcined powder was pressed into pellets ($d = 8$ mm) under a pressure of 200 MPa. Pressed pellets were sintered for 2 h at 1250 °C and in a water vapour atmosphere to avoid dehydration of OH^- from the HAp structure.

The synthesis of carbonate-containing amorphous calcium phosphate (cACP) was carried out by mixing phosphate and carbonate-containing solution (7.92 g $(\text{NH}_4)_2\text{HPO}_4$ and 0.96 g $(\text{NH}_4)_2\text{CO}_3$ dissolved in 250 mL deionized water), and calcium-containing solution (35.4 g $\text{Ca}(\text{NO}_3)_2 \cdot 4\text{H}_2\text{O}$ dissolved in 500 mL deionized water, which is mixed with 60 mL of concentrated NH_4OH). After mixing, the solution was stirred for 10 min and filtered on a Buchner funnel, rinsed with 2 L of deionized water and ammonia solution, finally rinsed with 250 mL of pure deionized water. After rinsing, the samples were placed in a freezer and frozen at -18 °C. After ~ 12 h, the frozen sample was lyophilized for 72 h in a vacuum at 0.01 mbar (at a condenser temperature of -90 °C).

The synthesis of cACP, additionally heated for 10 min at 480 °C to completely remove the tightly bound water without changing the amorphous phase [35], was used to produce dense ACP pellets by the spark plasma sintering (SPS) method. 0.3 g of cACP powder was placed in a 10 mm diameter graphite mould between thin graphite sheets and placed in the SPS equipment, where it was vacuumed at a pressure of 80 MPa for 30 min. The powder was heated to the final temperature with applied pressure (at a rate of 100 °C/min) and held for 10 min. Final temperatures of 200 °C, 500 °C and 700 °C were used to test the effect of temperature on pellet density.

Various analytical methods were used to characterize the samples: X-ray diffractometry (XRD), for determining phase composition of samples and evaluating crystal orientation;

Fourier transform infrared spectrometry (FTIR), for the determination of functional groups and the amount of OH⁻; scanning electron microscopy (SEM), for visual evaluation of surface properties and determination of grain size; atomic force microscopy (AFM) for topography measurement of individual thermally sprayed HAp droplets; and Raman spectroscopy, for determination of functional groups. Additional methods included density measurements, profilometry, determination of coating thickness, elemental analysis by inductively coupled plasma mass spectrometry (ICP-MS) and Ca/P determination by inductively coupled plasma optical emission spectrometry (ICP-OES). Additionally, data processing and analysis software were used – *Magic Plot Student 2.9* (for processing and deconvolution of spectra), *Origin2019* (for processing measurement data and design of figures), *Profex 4.3.6* (for Rietveld analysis), and *Spectra Gryph 1.2* (for processing the spectra).

Determination of OH⁻ ions in the amorphous phase

To examine the possibility of determining the amount of OH⁻ in the amorphous phase, crushed thermally sprayed low crystallinity CaP coatings were heated under vacuum (10⁻⁵ Torr) to 700 °C at different times (5–60 min), using a custom-made quartz system and quartz ampoules. After heating, the ampoules were melted closed, leaving the samples in closed ampoules, which were opened just before the analysis of the samples by FTIR KBr spectrometry.

Methods of creating and determining the surface charge

Polarization in an electric field was performed in a custom-made electric polarization system (see Fig. 2.1 a) by placing the samples between two platinum electrodes. The platinum electrodes were connected to a power supply. A clamp and a fibreglass insulation was used for complete electrode contact with the sample surface. Electric polarization was performed (in air) in an oven by heating the samples to the required polarization temperature for 1 h with an applied electric field, which was maintained until the samples cooled to the room temperature. After cooling, the electrodes were short-circuited to eliminate possible weekly bounded electric charges [36].

Custom-made set of TSDC measurement equipment was used to determine the generated surface charges by placing the sample between two Pt electrodes connected by Pt wires and insulated with a fibreglass layer (see Fig. 2.1 b). The Pt wires were insulated with Al₂O₃ ceramic tubes and connected to a current measurement device (picoammeter). The measurement cell was shielded with a metal grid and heated at a rate of 5 °C/min, the measurement was digitally read and a TSDC curve was obtained as a current versus temperature ratio. An external thermocouple was placed next to the measurement cell and used for temperature measurements.

Equation (1) was used to calculate the charge density from the TSDC curves.

$$Q_p = \frac{1}{\beta} \int_T^{\infty} J(T) dT, \quad (1)$$

where β is heating rate (°C/min) and $J(T)$ is current density, (nA/cm²). The integration was performed for the entire temperature measurement range.

Additionally, the depolarization activation energy was calculated from the TSDC curves (Equation (2)).

$$\frac{E_a}{\kappa T} + \ln \tau_0 = \ln \frac{1}{\beta} \int_T^\infty J(T) dT - \ln J(T), \quad (2)$$

where E_a is activation energy (eV), $J(T)$ is measured current density at temperature T , β is heating rate ($5^\circ\text{C}/\text{min}$), τ_0 is pre-exponential factor, and κ is Boltzmann's constant.

As an additional method for characterizing polarized HAp, contact angle measurements can be used, as the surface charge influences the surface wettability without changing the surface roughness or chemical compositions [37].

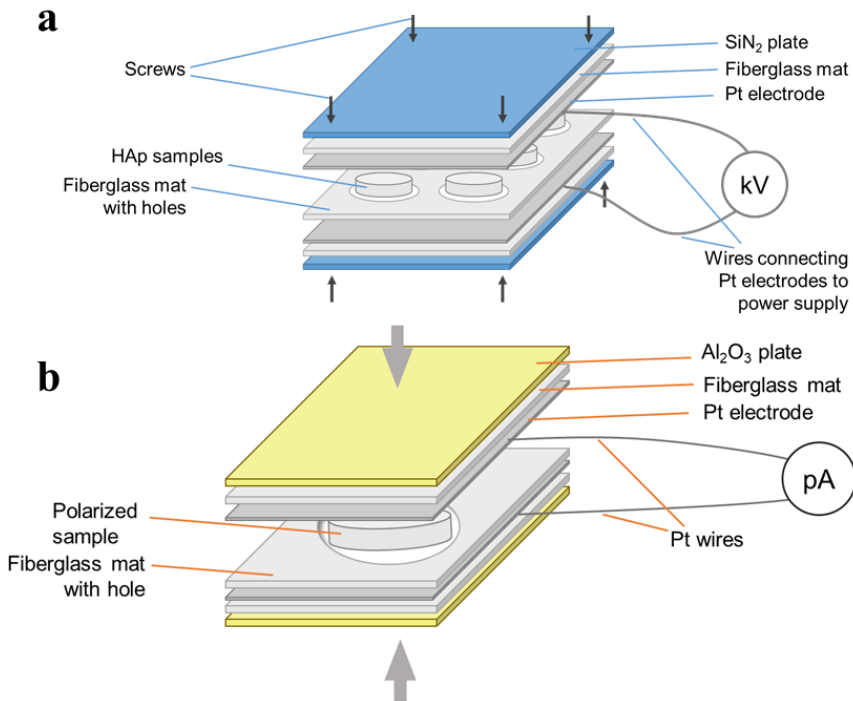


Fig. 2.1. Schematic representation of the polarization (a) and TSDC measurement cells (b) used in the study.

3. RESULTS AND DISCUSSION

3.1. Characterization of thermally sprayed hydroxyapatite droplets

To determine the most optimal parameters for the production of thermally sprayed coatings and to characterize the morphology of the particles obtained during spraying, individually sprayed HAp droplets were created and characterized. 3D images of the droplets were obtained with the AFM method, after which the geometry and morphology of the droplets were determined – spherical or with a pit (see Fig. 3.1). The droplet shapes indicated that the powder particles were completely melted because the centre itself was not uneven. The droplets expanded and returned to the centre of the droplet.

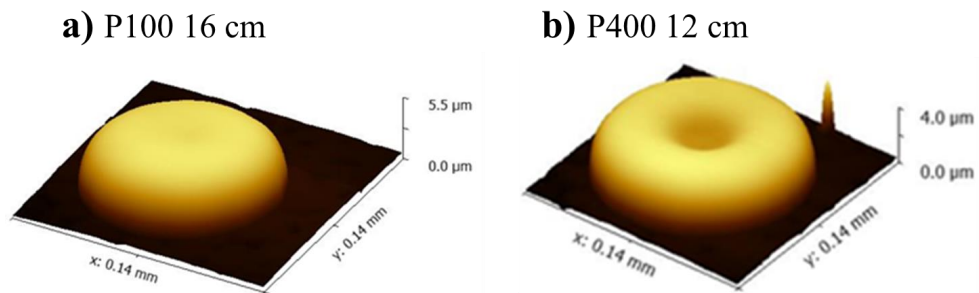


Fig. 3.1. AFM images of individual droplets: a) spherical droplet (no pit), b) droplet with small 12.7 μm pit.

Droplets with similar diameters were selected for further analysis. Looking at the shape of the droplets (see Table 3.1), for samples with a substrate temperature of 100 °C (P100), there are more droplets with pits at smaller spray distances, while at larger spray distances more droplets without pits appear. However, for samples with a 400 °C (P400) substrate, this relationship looks the other way around – at smaller distances (4 cm) droplets without pits are found.

Pits were formed from heat changes during droplet expansion. At a closer spray distance, there is less heat transfer in the droplet, and with a lower temperature, the molten droplet is not as fluid and cannot expand as much, so the height of the droplet will be higher. With a longer spray distance, there is a greater heat transfer from the flame to the powder particle – the formed droplet is more liquid, it expands more, indicated by a smaller height and a larger diameter. At a greater distance, the droplet has already started to cool down and a higher droplet was formed.

Comparing substrate temperatures – for P400 samples, droplets release heat more slowly at close spray distances. With slower cooling, the droplet does not solidify as quickly and begins to regain surface energy, reducing the droplet size. At P100 substrate, the upper layer of the droplet is unable to return to the centre of the droplet and the liquid forms a raised edge. There is more heat on the P400 substrate and as the droplet hardens more slowly, the liquid can return to the centre creating a flatter surface. It is important that on a substrate heated to 400 °C, droplets with a smaller well diameter were formed.

Table 3.1

Parameters of the selected droplets obtained from AFM measurements

Sample		Droplet characteristics					Pit diameter, μm	Pit depth, μm
		Diameter, μm	Volume, μm^3	Height, μm	Shape	Roughness, S_a [nm]		
100 °C	4 cm	108	28450	4.1	Pit	8	38.0	0.7
	8 cm	112	28980	4.3	Pit	8	39.0	0.8
		104	22560	3.3	Pit	8	47.0	0.6
	12 cm	116	28960	3.5	Pit	7	64.0	0.6
		116	29430	3.7	Pit	9	40.0	1.2
	16 cm	98	22590	4.6	Very small pit	7		0.3
		122	44160		Small pit	8		
	20 cm	96	30820	6.8	No pit	6		
102		26380	4.9	Pit	10	25.7	1.5	
400 °C	4 cm	110	27260	4.3	No pit	12		
		102	22860	3.5	No pit	12		
	12 cm	98	24110	3.7	Small pit	8	12.7	1.0
		114	28620	3.4	Pit	8	32.4	0.9
	20 cm	116	44440	5.4	No pit	30		
		116	39190	4.7	Pit	26		1.4

Unlike spraying individual droplets, coatings are formed when droplets overlap each other. In this case, droplet geometry is important. In order to prevent the formation of micro cracks between the droplets, it is necessary to find conditions in which droplets with small pits are formed. This can be observed for samples with substrate heated at 400 °C.

Individual droplets were analysed using Raman spectroscopy and compared to the spectra of the HAp spray powder (Fig. 3.2). Vibrational bands at 429 cm^{-1} and 446 cm^{-1} ($\nu_2 \text{PO}_4$); 578 cm^{-1} , 590 cm^{-1} , 606 cm^{-1} and 614 cm^{-1} ($\nu_4 \text{PO}_4$); 961 cm^{-1} ($\nu_1 \text{PO}_4$); 3572 cm^{-1} (OH) [38]–[40] were observed for the crystalline HAp spray powder. All spectra of droplets showed broadened phosphate vibrational bands ν_2 (~430 cm^{-1}), ν_4 (~596 cm^{-1}) and ν_1 (~950 cm^{-1}) [39], [41], but did not show the HAp characteristic PO_4 vibrational bands at 960 cm^{-1} and νOH^- band at 3572 cm^{-1} , which were detectable for the HAp spray powder. These deviations are a typical feature of amorphous calcium phosphate (ACP) [39], [42], indicating the amorphous nature of the droplets. It has been reported that the amorphous phase generally broadens the vibrational bands of HAp and enhances the low-frequency side of the bands [41]. The Raman spectra of all droplets showed the same trend and were comparable with each other.

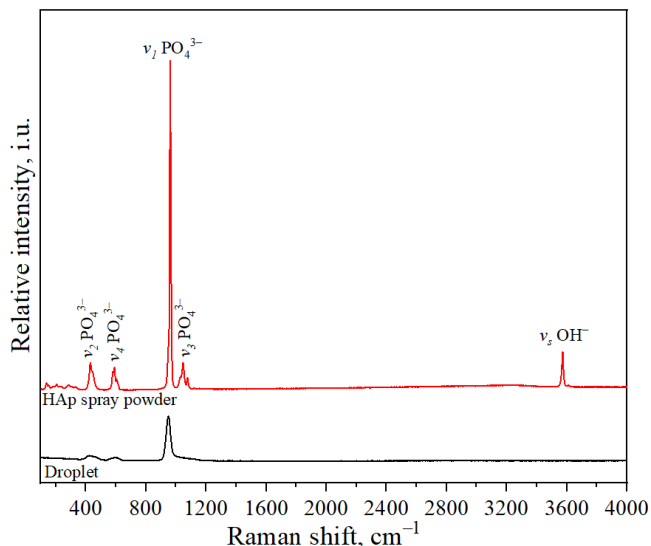


Fig. 3.2. Raman spectra of HAp spray powder and an individual droplet. Note the absence of the OH^- absorption peak in the droplet.

It was not possible to characterize the droplets individually with GIXRD. The measurement had to be taken over the entire sample area. But only for samples with a spray distance of 4 cm (both P100 and P400 samples) it was possible, because the samples with droplets sprayed from a greater distance had a lower droplet dispersion density on the sample surface. Therefore, only titanium peaks appeared in the X-ray diffraction.

Observing the obtained GIXRD data (Fig. 3.3) at a spraying distance of 4 cm, it can be seen that the samples show crystalline, lower intensity, and HAp (ICDD 01-074-0565) peaks, but more intense Ti (ICDD 04-001-8963) peaks. The most intense peaks are from Ti because the coating formed by the droplets is not thick enough to capture the more intense HAp X-ray

diffractions. It can be seen that the most intense peak of stoichiometric HAp (211) at 31.8° is no longer the most intense and has merged with the neighbouring HAp peaks at 32.2° and 32.9° (112 and 300). This trend of low intensity and merged peaks is characteristic of nanocrystalline apatite [43], [44], which was also formed by the presence of oxyapatite (OAp) and HAp. There are also other factors that complicate the interpretation. Given that the most intense Ti peak at 40.2° (101) overlaps with the HAp peak at 39.8° (130), it is suggested that it is the most intense HAp peak. At longer spraying distances it was no longer possible to detect the crystalline phase of HAp, but only Ti peaks corresponding to the substrate were detectable.

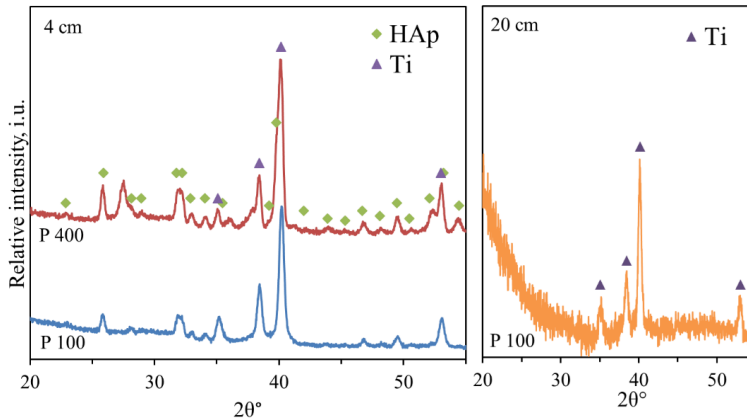


Fig. 3.3. XRD patterns of coatings sprayed at 4 cm (left) and 20 cm (right).

During the thermal spraying process of HAp, depending on the spraying distances (4–20 cm) and substrate heating temperatures (100 °C and 400 °C), it is possible to obtain droplets with different morphologies. It has been found that the most optimal form of thermally sprayed HAp droplets – droplets with a small pit – for the production of thermally sprayed coatings can be obtained at substrate heating of 400 °C.

3.2. Determination of OH⁻ ions in calcium phosphates

In this section, two studies are discussed – the incorporation of OH⁻ in thermally sprayed HAp coatings by the hydrothermal treatment and the determination of OH⁻ in amorphous calcium phosphate using a new technique.

3.2.1. Incorporation of OH⁻ ions into the HAp coating structure

During the thermal spray process of HAp, OH⁻ are removed and HAp undergoes partial decomposition into adjacent phases. Using the hydrothermal (HT) treatment, it is possible to introduce OH⁻ back into the HAp structure, which also allows the recrystallization of adjacent phases (e.g., OAp, TCP, TTCP, CaO, and ACP) formed during the thermal spray process. In HT treatment experiments, the effects of both temperature and time on the ability to incorporate

OH⁻ into the structure of thermally sprayed HAp were examined to find the most optimal HT processing parameters.

Initially, the sprayed HAp coating was analysed in comparison to the HAp spray powder by using XRD and FTIR analysis (Fig. 3.4). Coatings were scraped and crushed prior to analysis.

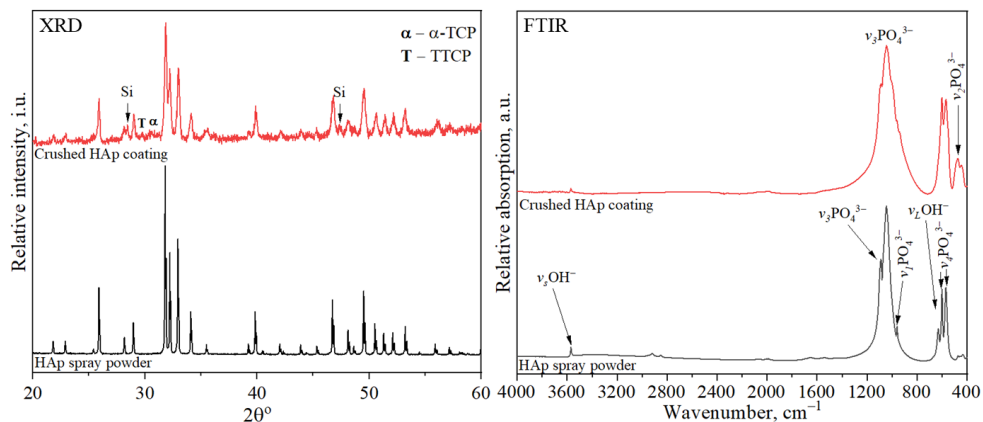


Fig. 3.4. XRD and FTIR comparison of HAp spray powder and crushed HAp coating.

As can be seen from the XRD results, more intense peaks are observed for the HAp spray powder, while the intensities of the crushed HAp coating are significantly lower. The silicon (Si) peak is from the sample cuvette. The Rietveld method (*Profex 4.3.6* [45]) and the structure database were used for the quantitative determination of the phase composition. Rietveld analysis of the HAp spray powder showed a 100 % HAp phase. The determined crystallite sizes showed a high crystallinity of 254 ± 6 nm (in the 001 dimension or along the c-axis) and 284 ± 9 nm (in the 100 dimension along the a-axis). However, XRD of the crushed HAp coating showed 69 % of HAp with crystallite sizes of 299 ± 38 nm (001) and several impurity phases – OAp (14 %), TTCP (12 %), and α -TCP (5 %), indicating the thermal decomposition due to high spray temperature [46]–[48]. Previous studies have shown that TCP and TTCP phases are observed in larger amounts when higher heat transfer to the particle dominates [47], which in this case is provided by substrate heating.

A deeper understanding of the formation of HAp chemical bonds was obtained by FTIR spectrometry. Spectrum of HAp spray powder was characteristic of HAp showing PO_4^{3-} apatitic absorption bands at 472 cm^{-1} (ν_2), 561 cm^{-1} , 574 cm^{-1} and 602 cm^{-1} (ν_4), 960 cm^{-1} (ν_1), 1032 cm^{-1} , 1046 cm^{-1} and 1087 cm^{-1} (ν_3); absorption bands at 631 cm^{-1} and 3572 cm^{-1} are characteristic of apatitic OH⁻ bands [49], [50]. While the crushed HAp coating does not show a clearly distinguishable OH⁻ absorption band at 631 cm^{-1} and the band at 3572 cm^{-1} is of lower intensity, indicating dehydroxylation (loss of OH⁻) after thermal spraying [51].

HT treatment of HAp coatings was performed at $200 \text{ }^\circ\text{C}$ at different times (6 h, 12 h, 24 h, and 48 h) and FTIR spectra were taken. For the quantification of OH⁻, the method developed by L. Plūduma was used [52], by deconvolution of FTIR spectra (before and after HT treatment) at the $500\text{--}700 \text{ cm}^{-1}$ spectral region with 6 Lorentz distribution bands (Fig. 3.5).

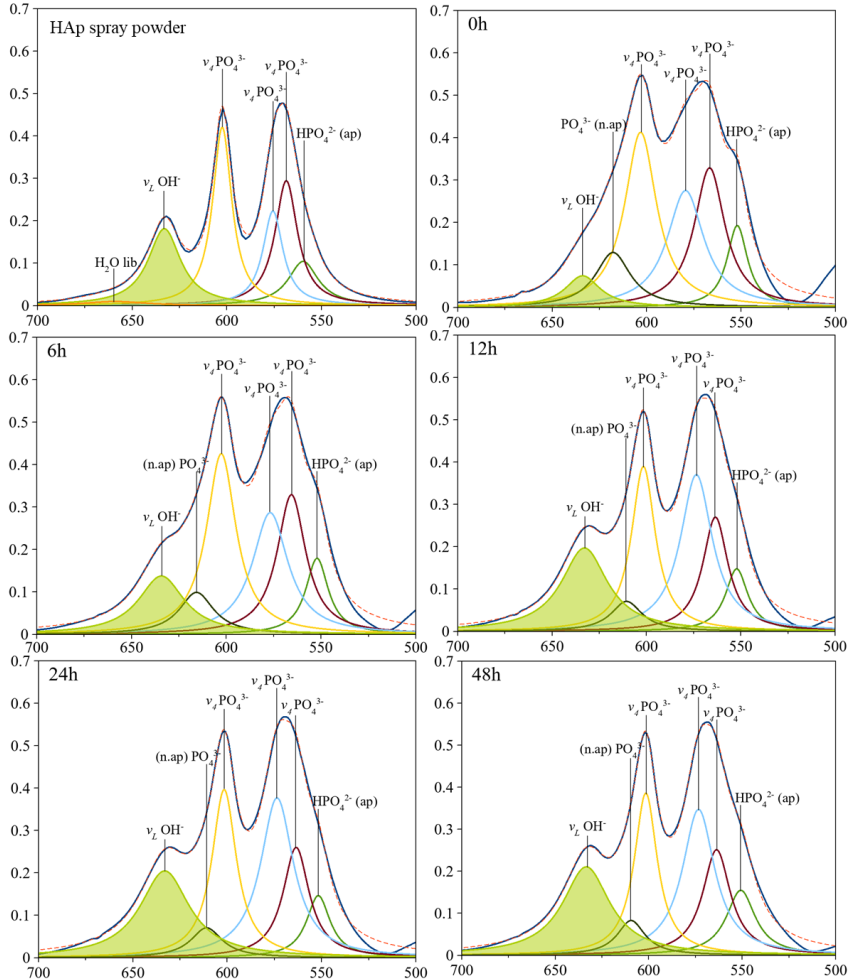


Fig. 3.5. Deconvolution of FTIR spectra of HAp coatings before and after HT treatment.

The spray powder was not stoichiometric HAp, as an apatitic HPO_4^{2-} absorption band at $\sim 550 \text{ cm}^{-1}$ was determined, and a libration band of H_2O absorption band at $\sim 670 \text{ cm}^{-1}$ was also identified, associated with water molecules attached to the surface [43], [53]. The HAp spray powder did not show the non-apatitic PO_4^{3-} absorption band at $\sim 617 \text{ cm}^{-1}$, which is typically characteristic of nanocrystalline and non-stoichiometric apatites [43]. However, for HAp coating both before and after HT treatment at different times, absorption band of non-apatitic PO_4^{3-} absorption band was observed, which indicates the non-stoichiometry of the material, as well as impurities of other calcium phosphate phases (TTCP and α -TCP).

From the spectral deconvolution, the percentage of OH^- was calculated, which is shown in Fig. 3.6, and shows the change of OH^- in an oriented HAp coating before and after HT treatment at $200 \text{ }^\circ\text{C}$. It can be seen that the HAp spray powder used does not have 100 % OH^- content comparing to the standard HAp (100 %) used in the OH^- calculations. This is explained by the

manufacturing process of HAp spray powder. Increasing the HT treatment time also increases the incorporated OH^- content until it reaches its maximum after 24 h ($88 \pm 6\%$) and remains unchanged even after 48 h of HT treatment ($85 \pm 6\%$). This leads to the conclusion that the maximum amount of OH^- that can be incorporated in thermally sprayed coatings does not reach 100%. Taking into account these experiments, further HT processing of HAp coatings were carried out at 250°C for 12 h – by increasing the HT processing temperature, but by optimizing the time it was possible to obtain HAp coatings with an equivalent amount of OH^- ($75 \pm 5\%$).

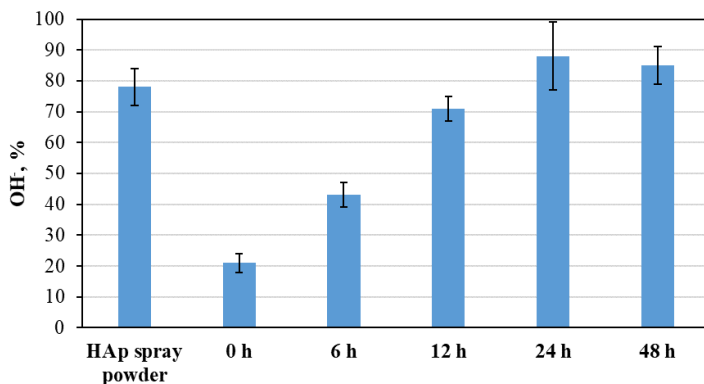


Fig. 3.6. Changes of OH^- in the HAp coating before and after HT treatment at 200°C .

During the HT treatment, needle-like HAp crystals are formed on the surface of the HAp coating, which are characteristic of crystallization by the HT treatment [54], [55] and can be observed in SEM images (Fig. 3.7).

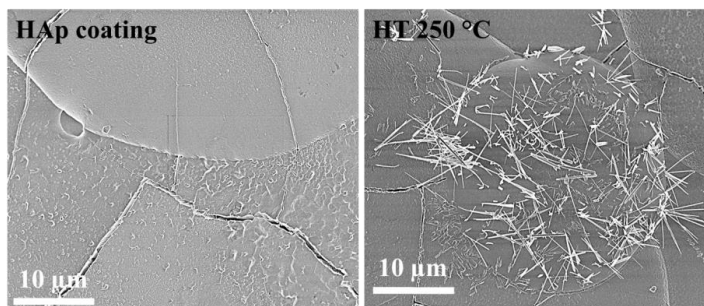


Fig. 3.7. SEM images of HAp coating before and after HT treatment at 250°C for 12 h.

HAp loses about 73% OH^- during thermal spraying, which can be returned up to $88 \pm 6\%$ to the HAp coating by HT steam treatment and reduce the amount of decomposition phases formed during thermal spraying.

3.2.2. Characterization of OH^- ions in the amorphous phase using a new technique

In this study, vacuum heating of ACP was considered to determine the amount of OH^- in the amorphous phase. The study is based on the possibility of determining OH^- in the apatite

structure by FTIR spectroscopy both at 631 cm^{-1} (ν_L OH⁻ libration mode) and at 3572 cm^{-1} (ν_s OH⁻ stretching mode). When HAp powder is introduced into a flame or plasma, the first material loss is the removal of OH⁻ from the structure in the form of water [56]. Loss of OH⁻ originates from the outside of the molten powder droplet and progresses deeper into the powder particle following the established pattern [47], remaining in the core of the droplet itself. When the droplet contacts the substrate surface, the droplet expands to form a “pancake” shape, which promotes rapid cooling of the droplet, solidifying it to form an amorphous phase. The absence of OH⁻ takes away an important part for the formation of crystals, which also contributes to the formation of the amorphous phase. These factors simultaneously inhibit crystallization.

A thermally sprayed low-crystallinity CaP coating was used for the implementation of the study. Although a completely amorphous phase was not obtained and XRD indicated impurities of crystalline phases, which traditionally limits further investigation, however, a new approach was proposed in this study to be able to obtain more information about the chemical content of the thermally sprayed HAp powder.

The amorphous phase does not structurally hold the OH⁻ in a position that can be absorbed by infrared light to indicate the presence of OH⁻. This study proposes an approach to learn about the existence of OH⁻ in the amorphous phase by crystallizing the amorphous phase in vacuum, which could incorporate the OH⁻ into the lattice where they would be able to absorb light (FTIR) and indicate the existence of OH⁻.

After heating in vacuum, FTIR spectra of the samples were taken in a KBr matrix (see Fig. 3.8). In the FTIR spectra of low-crystallinity CaP coatings both before and after heating in vacuum at different times, the characteristic absorption bands of OH⁻ at 631 cm^{-1} (ν_L) and at 3572 cm^{-1} (ν_s) were not detectable. On the other hand, for commercial HAp, these OH⁻ absorption bands are clearly visible both before and after heating in vacuum for 60 min. This indicates the stability of crystalline HAp powder after heating in vacuum. The vacuum-heated low-crystallinity CaP coating shows a different spectrum – the characteristic absorption bands of PO₄³⁻ at 566 cm^{-1} and 604 cm^{-1} (ν_4) are visible, but several absorption bands overlap in the spectral region of ν_1 PO₄³⁻ and ν_3 PO₄³⁻ ($\sim 700\text{--}1700\text{ cm}^{-1}$), which are not characteristic of HAp. Comparing the CaP coatings with low-crystallinity heated for 5 and 10 min with those heated for 60 min, it can be seen that after 5 and 10 min of heating more water remained – absorption band at $3000\text{--}3800\text{ cm}^{-1}$ and ν_4 PO₄³⁻ spectral region ($525\text{--}700\text{ cm}^{-1}$) show more merged absorption bands, indicating lower crystallinity.

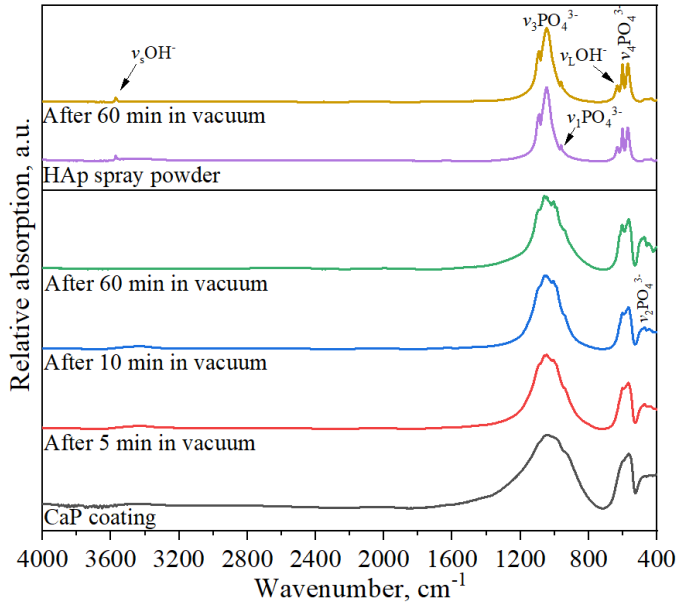


Fig. 3.8. Comparison of FTIR spectra of low-crystallinity CaP coating and crystalline HAp before and after heating in vacuum (10^{-5} Torr).

XRD was taken for the low-crystallinity CaP coating before and after heating (60 min at 700 °C) in vacuum and it was observed that the amorphous phase has crystallized, as the broad amorphous peak that was observed before heating in vacuum was no longer observed (Fig. 3.9).

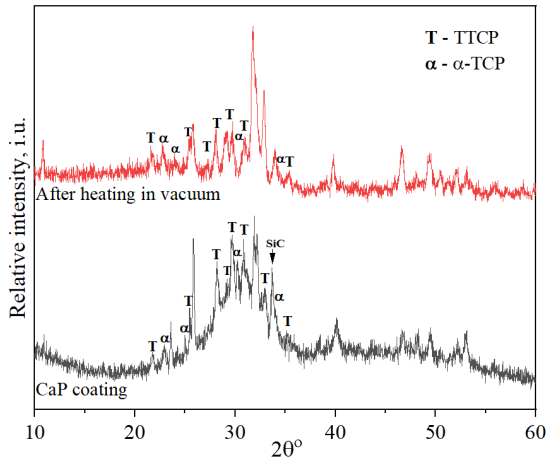


Fig. 3.9. XRD of low-crystallinity CaP coating before and after heating (60 min at 700 °C) in vacuum (10^{-5} Torr).

Rietveld analysis was performed on both samples to determine the phase composition (Fig. 3.10). XRD was taken for the coating before heating in vacuum and for the crushed

coating after heating in vacuum. Before heating in vacuum, the phase content was determined only for the crystalline part without taking into account the amorphous background.

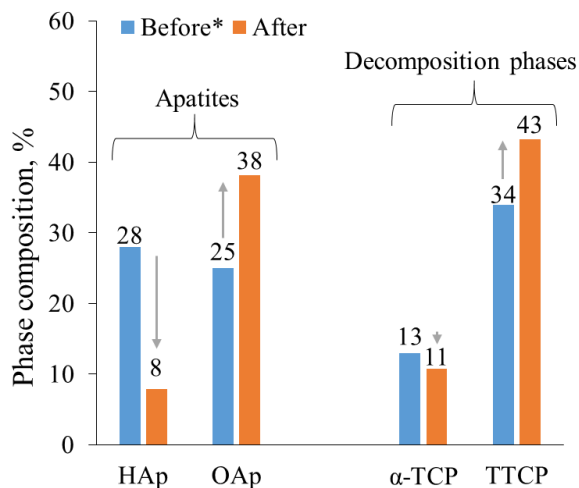


Fig. 3.10. Rietveld analysis results of the crystalline phase for low-crystallinity CaP coating before and after heating (60 min at 700 °C) in vacuum. *The phase content is shown for the crystalline part before heating in vacuum.

It can be seen that after vacuum heating, the amount of TTCP and OAp increased, while HAp decreased. No major changes in the content of the α -TCP phase were observed, indicating its stability under the given heating conditions.

In order to determine more precise changes after heating in vacuum, deconvolution of the absorption bands of the ν_4 PO_4^{3-} spectral region (525–700 cm^{-1}) was performed (Fig. 3.11), identifying the OH^- absorption band at ~ 632 cm^{-1} , which is otherwise overshadowed by the adjacent phosphate absorption bands. The OH^- absorption band in the amorphous phase before heating in a vacuum is relatively pronounced, but as the heating time at 700 °C increases, its intensity visibly decreases.

After deconvolution, the areas of the absorption bands were calculated, from which the amounts of OH^- were calculated: 35 ± 6 % (prior heating), 15 ± 0.3 % (after 5 min), 10 ± 6 % (after 10 min) and 2 ± 2 % (after 60 min).

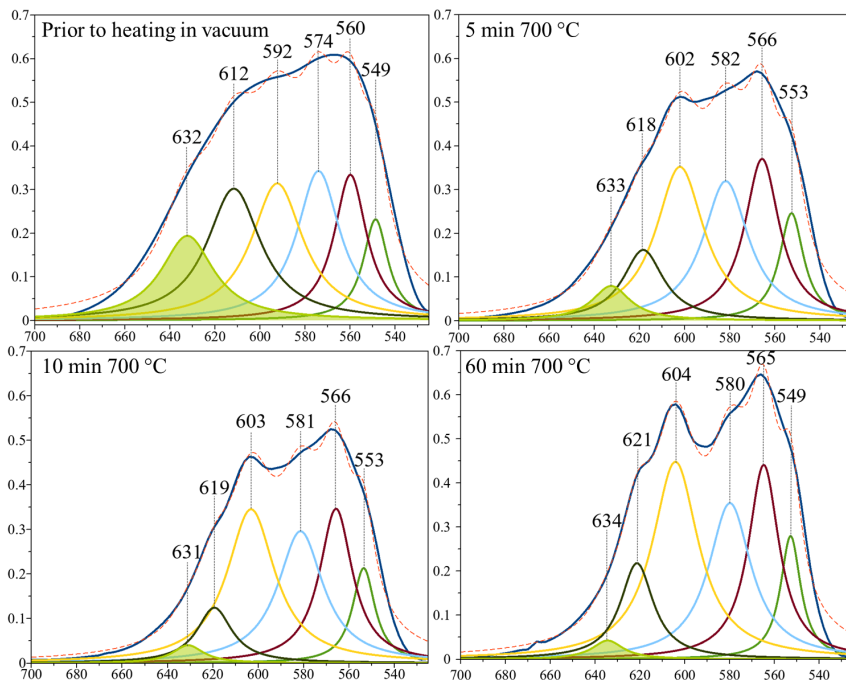


Fig. 3.11. Deconvolution of the FTIR absorption bands of the low-crystallinity CaP coating before and after heating in vacuum.

A shift of absorption bands to higher wavenumbers was observed with increasing the heating time in vacuum. Previous studies have shown the following trend where the OH⁻ absorption band shifts to higher wavenumbers for samples with lower OH⁻ content [57], when the OHAp phase is formed. Such absorption band shifts and band broadening are characteristic of nanocrystalline apatites [58]. The shift of the absorption band at 574 cm⁻¹ to a higher wavenumbers at ~580 cm⁻¹ may indicate the presence of impurity phases TTCP and α -TCP [59].

An initial hypothesis for the determination of OH⁻ in the amorphous phase was the rapid ordering to the crystalline structure after heating in vacuum at 700 °C. To test the crystallization rate, the sprayed low-crystallinity CaP coating and, as a comparison, a synthesized carbonate containing amorphous calcium phosphate (cACP) to further stabilize the amorphous phase, were heated under vacuum. FTIR spectra were recorded for these samples (Fig. 3.12). It was initially predicted that sprayed ACP phase would crystallize faster, while CO₃-enriched synthesized cACP would crystallize more slowly. However, the results showed the exact opposite result – the thermally sprayed ACP phase crystallized much more slowly.

Faster crystallization of cACP compared to thermally sprayed low-crystallinity CaP coating can be explained by hard-to-remove water molecules around Posner clusters in the cACP structure [3], [35], which contribute to faster crystallization. Free water molecules were still present in the sample heated to 700 °C, indicating that it was difficult to remove. While in the thermally sprayed amorphous phase, the chemical content changes when the sample is at the

flame and the crystallization process is much more complicated than ion reorientation for synthesized cACP.

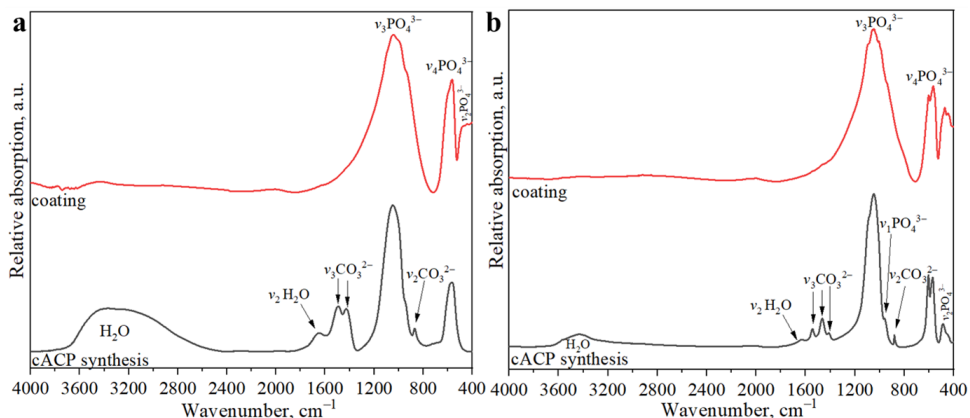


Fig. 3.12. FTIR spectra of two types of ACP before (a) and after (b) heating at 700 °C.

The hypothesis of the possibility of determining the amount of OH⁻ in the thermally sprayed crystallized amorphous phase is only partially confirmed because instead of HAp the sprayed coating also included the presence of different calcium phosphate phases (TTCP, OAp, α -TCP), however, the method shows trends in OH⁻ changes.

3.3. Measurement of surface charges

It is possible to create a surface charge on calcium phosphates by polarizing them in an electric field. In the Thesis the method of formation of surface charges of various calcium phosphate samples and the determination of these charges using the thermally stimulated depolarization current (TSDC) was used.

3.3.1. Inter-laboratory study of electrical polarization and TSDC measurements

For the creation of electric charges with electric polarization and for the determination of charges, using the TSDC method, custom-made sets of equipment were created, based on the information found in the literature. To verify the repeatability of these methods, an inter-laboratory study was conducted between laboratories in Riga (Institute of Materials and Surface Engineering, RTU) and Tokyo (Institute of Biomaterials and Bioengineering, Tokyo Medical and Dental University).

HAp pellets with high relative density (97.1 ± 0.4 %), made in the same way (in Tokyo) were used for the study and were polarized and depolarized in each of the laboratories. Before measuring the HAp pellets, an in-depth analysis of the samples was performed. XRD of sintered HAp pellets (Fig. 3.13 a) showed HAp (ICDD 01-074-0565) and OAp (ICDD 04-011-1880) phases. Rietveld analysis showed a phase composition of 87 % (HAp) and 13 % (OAp), indicating the formation of an adjacent phase after sintering, despite the fact that sintering was

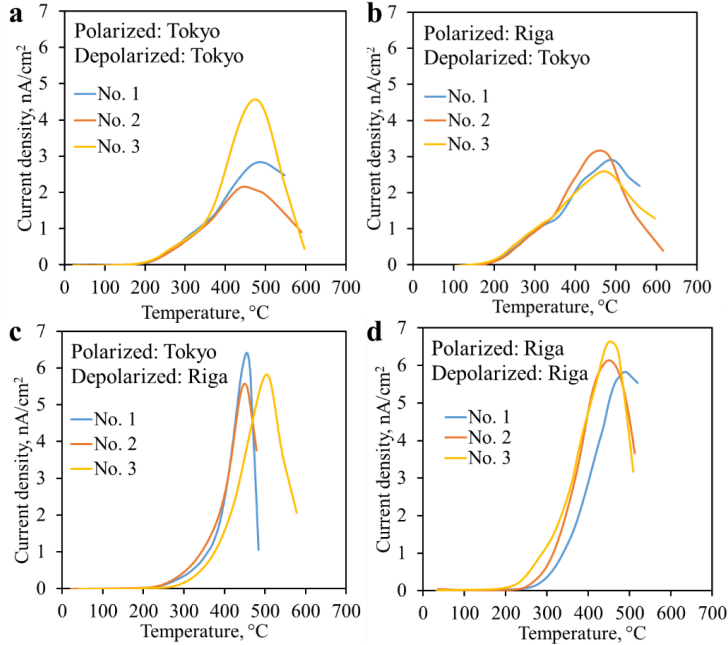


Fig. 3.14. TSDC results for HAp ceramics polarized and depolarized in two laboratories.

The parameters calculated from the TSDC curves are summarized in Table 3.2. The mean charge densities are quite close and within the error limits. The set of measurements performed in Riga (polarized and depolarized) show higher values of surface charges compared to other measurement series.

Table 3.2

Results calculated from TSDC curves

	Current density, nA/cm²	At temperature, °C	Charge density, μC/cm²	Activation energy, eV
Pol./depol. Tokyo	3.2 ± 1.2	472 ± 20	6.0 ± 1.6	0.69 ± 0.04
Pol. Riga – depol. Tokyo	2.9 ± 0.3	475 ± 19	6.3 ± 0.2	0.71 ± 0.02
Pol. Tokyo – depol. Riga	5.9 ± 0.4	470 ± 32	6.4 ± 1.2	0.74 ± 0.03
Pol./depol. Riga	6.2 ± 0.4	457 ± 23	9.0 ± 1.4	0.72 ± 0.01

TSDC curves obtained in Tokyo are wider, while in Riga – narrower but with higher current density peaks. When looking at each series individually, it can be observed that the TSDC curves have similar trends and the measurements do not differ drastically, only in some cases, slightly different peak positions can be observed (in Fig. 3.14 a – peak No. 3, c – peak No. 3, d – peak No. 1). The standard deviations of the charge density measurements indicate a good repeatability of the measurements. On average, the highest charge densities were obtained for samples polarized and depolarized in Riga – $9.0 \pm 1.4 \mu\text{C}/\text{cm}^2$, while the lowest charge densities were obtained for samples polarized and depolarized in Tokyo – $6.0 \pm 1.6 \mu\text{C}/\text{cm}^2$.

The activation energies ranged from 0.69 to 0.74 eV and were attributed to proton conduction, as reported in previous studies [34], [60]. It should be noted that the activation energy does not depend on the grain size, while the surface charge density is greatly affected by the grain size [32].

The small difference in the results could also be explained by the influence of other factors on the polarization and TSDC measurements, such as room temperature, air humidity, external electromagnetic fields and sample storage conditions. Although previous studies have shown that the surface charge of HAp does not change over time [13], [61], it could be argued that fluctuations in the surrounding environment could slightly affect the stored surface charge. Temperature and humidity at the time of measurement can affect surface charge measurements. Higher humidity can lead to higher current measurements than in a dry environment [62], because humidity makes the air more conductive, allowing for a more even distribution of excess charges.

This study was conducted to provide a comparison between different laboratories and slightly different environmental factors to evaluate the accuracy of the methods. Despite slightly different results, it can be seen that both charge densities and activation energies are within the error limits. In conclusion, the chosen TSDC method has a sufficiently high accuracy, considering that the equipment used in the two laboratories also differed, and this repeatability is accurate enough to be able to compare different types of samples.

3.3.2. Surface charge measurements on SPS pellets

For spark plasma sintering (SPS) pellets were made from carbonate-containing amorphous calcium phosphate (cACP) powder. Pellets were made at 3 different sintering temperatures – 200 °C, 500 °C and 700 °C (hereinafter SPS-200, SPS-500 and SPS-700). This type of synthesis was chosen in order to be able to compare with experiments carried out in other laboratories [63], [64].

The synthesized cACP powder and SPS pellets showed an amorphous structure at temperatures below the crystallization temperature of HAp (SPS-200 and SPS-500), while above the crystallization temperature, the pellets were crystalline (SPS-700), as determined by XRD measurements (Fig. 3.15 a). Both A-type (ICDD 04-011-0242) and B-type (ICDD 04-016-7498) carbonate apatite (CHAp) phases were identified for crystalline SPS-700 pellets.

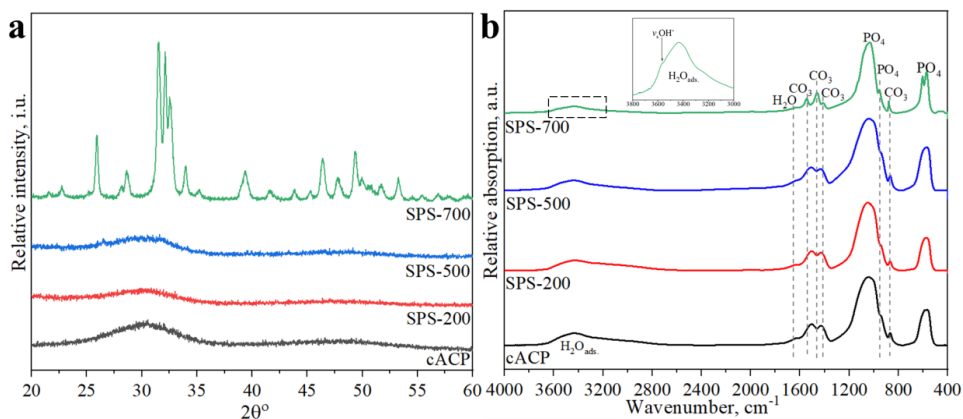


Fig. 3.15. XRD (a) and FTIR spectra (b) of pellets made with SPS.

As can be seen from the FTIR spectra (Fig. 3.15 b), amorphous samples (cACP, SPS-200 and SPS-500) show broad PO_4^{3-} absorption bands at 1040 cm^{-1} (ν_3), 949 cm^{-1} (ν_1) and 560 cm^{-1} (ν_4), CO_3^{2-} at 1500 cm^{-1} (ν_3), 1430 cm^{-1} (ν_1) and 866 cm^{-1} (ν_2), and a broad H_2O absorption band at 3400 cm^{-1} and 1630 (ν_2) [38], [49], [63], which are characteristic of amorphous carbonate apatite.

FTIR spectrum of a crystalline sample (SPS-700) shows much better resolved PO_4^{3-} absorption bands at $1020\text{--}1120\text{ cm}^{-1}$ (ν_3), 962 cm^{-1} (ν_1), 602 cm^{-1} and 574 cm^{-1} (ν_4), corresponding to calcium phosphate apatite, confirming crystallization from the amorphous phase to the apatite phase [38], [49], [63]. The broad water absorption bands at 3400 cm^{-1} and 1630 cm^{-1} (ν_2) have much lower intensity than the amorphous samples. The CO_3^{2-} vibration bands at 1542 cm^{-1} and 878 cm^{-1} correspond to A-type carbonate apatite, while the bands at 1462 cm^{-1} and 1412 cm^{-1} correspond to B-type carbonate apatite [38], [63], thus confirming the formation of AB-type carbonate apatite.

For in-depth analysis of FTIR spectra, the deconvolution of $\nu_2\text{ CO}_3^{2-}$ absorption bands in the $800\text{--}900\text{ cm}^{-1}$ spectral region was used (Fig. 3.16), which showed the inclusion of various carbonates in the apatite structure. Deconvolution of the $\nu_2\text{ CO}_3^{2-}$ spectral region is used to identify changes in carbonate content that are incorporated into the apatite structure [65]. The two main carbonate bands of bone apatite are located at 878 cm^{-1} (A-type) and 871 cm^{-1} (B-type), however, slight shifts of the absorption bands are possible in mixed-type carbonate apatites, attributed to small changes in lattice dimensions due to substituent ions. The third absorption band identified corresponds to non-apatite carbonate ($\sim 866\text{ cm}^{-1}$) and appears, as a “shoulder” in the crystalline sample (SPS-700), but with a slight shift to lower wavenumbers is detectable in the amorphous samples. This absorption band decreases with increasing crystallinity of the sample and is usually only observed in nanocrystalline apatites and bone [58], [66]. In previous studies, this non-apatitic carbonate absorption band has decreased upon crystallization of carbonate apatites, thus allowing for greater incorporation of carbonate into the apatite lattice, favouring the phosphate site (B-type) [65].

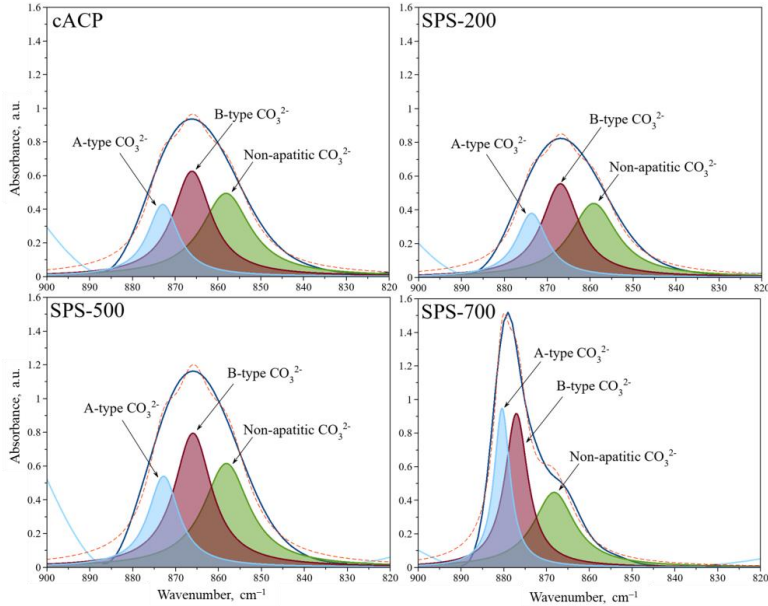


Fig. 3.16. Deconvolution of FTIR spectra in $\nu_2 \text{CO}_3^{2-}$ absorption region.

The surface charge densities of SPS pellets were determined by TSDC curves (Fig. 3.17), after polarization in an electric field of 1 kV/cm at 400 °C for 1 h. The TSDC curves for the amorphous samples started to develop at about 265 °C and reached their maximum at 455 °C (SPS-200) and 476 °C (SPS-500), while for the crystalline (SPS-700) charge release started to show already at ~200 °C and reached peak at 482 °C. The lower charge release temperature also coincides with the lower activation energy (E_a), which was 0.6 eV for the SPS-700 sample, while the amorphous SPS-200 and SPS-500 samples had E_a of 1.3 eV and 0.9 eV, respectively. This suggests that more energy was required to release the charge in the ACP samples. $E_a \sim 0.70$ eV is characteristic of proton conduction [67], while higher $E_a > 1$ eV are characteristic of space charge polarization arising from long-range proton conduction between grain boundaries [34]. In the ACP samples, the high activation energies could also be related to migration of O^{2-} [68]. However, these described processes are specific to crystalline Hap, and there is a lack of information about possible processes in the amorphous phase.

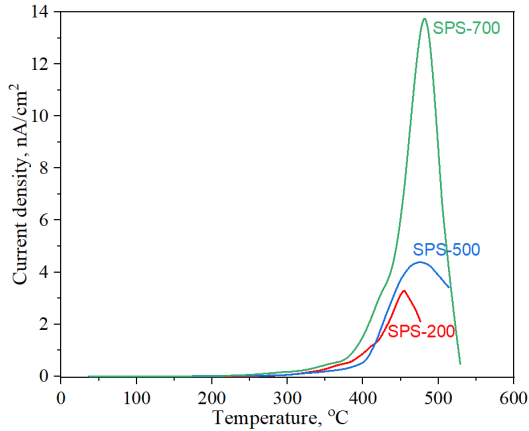


Fig. 3.17. TSDC curves of SPS pellets after polarization in an electric field.

By increasing the sintering temperature it was possible to obtain samples with a higher density, in this way pellets with a higher density also showed a higher surface charge density (Table 3.3). The effect of density is addressed in studies with crystalline HAp ceramics, showing a higher charge density for samples sintered at higher temperatures [69]. However, as sintering temperatures increase, grain sizes also increase, which is considered to be one of the crucial factors for increasing the surface charge. This can be explained by the effect of the grain boundary on dipole formation in HAp ceramics due to the high ionic conduction resistance of the grain boundary, which acts as an inhibitor of proton migration [32].

Table 3.3

Structural characteristics and stored charge of SPS pellets

Sample	Density of pellet, g/cm ³	Max. current density, nA/cm ²	At temperature, °C	Charge density, μC/cm ²	Activation energy, eV
SPS-200	1.24 ± 0.03	3.3	455	2.3	1.3
SPS-500	1.55 ± 0.07	4.4	476	4.5	0.9
SPS-700	1.84 ± 0.05	13.8	482	10.4	0.6

The maximum relative density of crystalline pellet (SPS-700) is only 58 %, which is much lower than, for example, the pellets used in the previous inter-laboratory study. However, a higher average charge density was obtained for the SPS-700 sample compared to the HAp used in the inter-laboratory study. This suggests that the effect of pellet density on the created surface charge is smaller and the composition of the samples is probably more important. SPS samples contained CHAp and carbonate substitution in the HAp structure has previously shown a significant increase in charge densities compared to unsubstituted HAp [70], [71]. Thus, CHAp is a desirable combination not only for fabricating high-efficiency implants, but also for fabricating electrets with high polarization capacity.

This is the first known study to date on the creation and detection of ACP surface charge. According to the results of this study, it can be concluded that amorphous calcium phosphates can also form surface charges, which can then be determined by the TSDC method. The formation of lower charges suggests that dipole orientation is the main mechanism that promotes the formation of surface charges.

3.3.3. Effect of polarization temperature on the magnitude of the surface charge

Surface charge generation and determination has previously been performed on stoichiometric HAp coatings and sintered pellets, but this study examines electric charge generation on HAp coatings with a $\langle 001 \rangle$ oriented crystal structure. The crystal orientation is obtained in the thermal spraying process, when the particles of spray powder melted in the flame lay on the surface of a preheated (400 °C) substrate, which does not allow them to cool down so quickly and the crystal growth takes place in the direction of the fastest heat dissipation, forming the $\langle 001 \rangle$ crystal orientation [72], [73]. Crystal orientation was determined by XRD (Fig. 3.18), where two distinct diffraction peaks at 25.9 $2\theta^\circ$ and 53.2 $2\theta^\circ$ were observed, which correspond to peaks in the (002) and (004) plane [46], [72]. The other peaks are missing because there are no crystals with the necessary orientation to allow the X-ray to diffract.

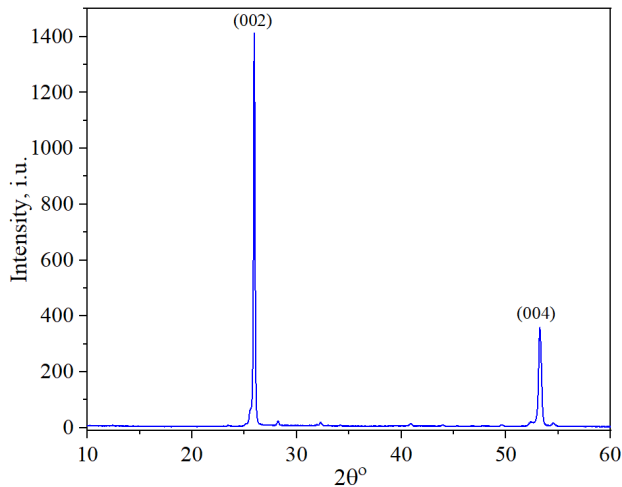


Fig. 3.18. XRD of hydroxyapatite coating with oriented crystals.

The effect of polarization temperature on oriented HAp coatings was performed by electrically polarizing the coatings at different temperatures ($T_p = 300 - 450$ °C) at a constant electric field ($E_p = 10$ kV/cm) and holding time ($t_p = 1$ h). As the polarization temperature increased, the intensity of the recorded TSDC curves increased (Fig. 3.18), which indicates an increase in the size of the surface charge.

According to the inset in Fig. 3.19, it can be seen that the first rise appears slightly before 100 °C and is attributed to the orientation polarization of the absorbed water [32], which gives the lowest contribution to the charge magnitude and the fastest dipole relaxation time.

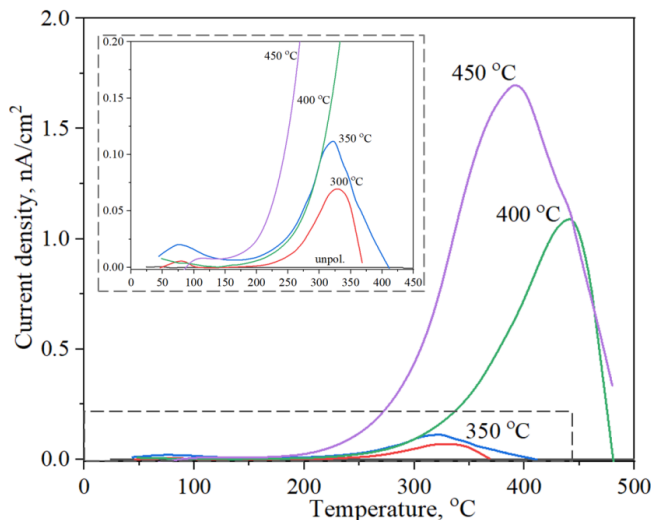


Fig. 3.19. TSDC curves after electrical polarization of HAp coating with oriented crystals.

The electrical polarization temperature is known to be the determining factor in controlling the properties of sintered HAp electrets, as the protonic conductivity changes exponentially with temperature [32]. The same trend can be observed in this case, when oriented HAp coatings are polarized at different temperatures. Based on the TSDC curves, the surface charge values were calculated (Fig. 3.20 a), which varied from 0.06 $\mu\text{C}/\text{cm}^2$ to 2,6 $\mu\text{C}/\text{cm}^2$. However, the activation energies (Fig. 3.20 b) did not differ significantly at different polarization temperatures and were within the range of 0.67 eV, indicating its independence from the polarization temperature.

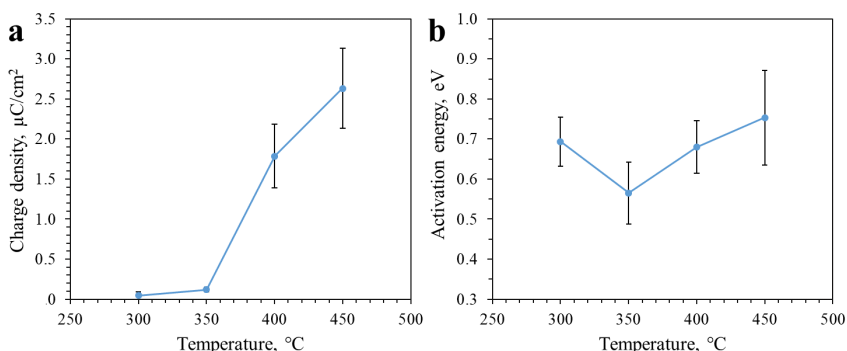


Fig. 3.20. The effect of polarization temperature on the surface charge (a) and activation energy (b).

After this study, the following electric polarization parameters were chosen: 400 °C for 1 h and 10 kV/cm. A polarization temperature of 400 °C was chosen to provide the most optimal and comparable results between different coatings.

3.3.4. Surface charge of apatite coatings of different structures

In order to compare how the structure of the apatite coating affects the surface charge, a comparison of these coatings was made by polarizing different coatings in an electric field:

- ✓ HAp coating with oriented crystal structure (with low OH⁻ content, 21 ± 3 % OH⁻);
- ✓ HT treated HAp coating with oriented crystal structure (with high OH⁻ content, 75 ± 5 % OH⁻);
- ✓ HAp coating with random crystal orientation (HT treated low-crystallinity CaP coating);
- ✓ Low-crystallinity CaP coating.

Polarization experiments were performed for all types of coating at the same parameters – $E_p = 10$ kV/cm, $T_p = 400$ °C, and $t_p = 1$ h. A comparison of the obtained TSDC curves for samples with different crystal structures are shown in Fig. 3.21.

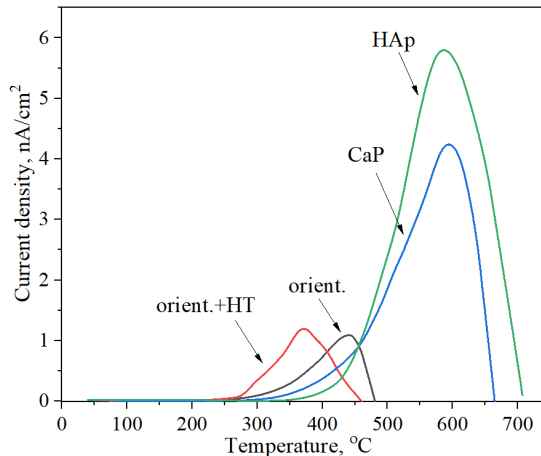


Fig. 3.21. TSDC measurements of apatite coatings with different structures.

Average calculated surface charge densities were slightly higher for the oriented HAp coating ($1.8 \pm 0.7 \mu\text{C}/\text{cm}^2$) compared to the HT treated coating ($1.6 \pm 0.1 \mu\text{C}/\text{cm}^2$). This indicates that the incorporation of OH⁻ into the structure of the thermally sputtered coating did not provide additional charge storage capacity. The activation energies for oriented HAp coating after HT treatment decreased from 0.69 eV (before HT treatment) to 0.59 eV. However, this reduction is not significant.

Low-crystallinity CaP coating and randomly oriented HAp coating (HT treated crystallized low-crystallinity CaP coating) showed much higher surface charge than coatings with oriented crystal structure. Comparing the low-crystalline CaP coating with the HAp coating shows that the crystalline HAp coating has a higher charge density ($10.9 \mu\text{C}/\text{cm}^2$) compared to the low-crystallinity CaP coating ($8.1 \pm 2.0 \mu\text{C}/\text{cm}^2$). This indicates that the randomly oriented HAp

structure exhibits the highest charging capacity of all the structures considered. This could be explained by the crystal structure itself, where an oriented crystal structure is designed in such a way that it is more difficult to form a charge than in a randomly oriented structure. On the other hand, the activation energy for the low-crystallinity CaP coating after crystallization increased significantly compared to the non-crystallized coating from 0.91 eV to 1.49 eV. This suggests a higher energy requirement for dipole relaxation in the material. Higher activation energies have been shown for electrically polarized tricalcium phosphate ceramics at more intense polarization conditions [36], explained by deeper activated grain boundaries. In this study, a relatively high electric field (10 kV/cm) was used, which has also been previously indicated that increasing of the polarization field shifts the TSDC peaks to higher temperatures [68], which also affects the magnitude of the calculated activation energy.

3.3.5. Effect of surface charge on the contact angle of apatite coatings of different structures

Electrical polarization is able to affect the surface wettability and surface energy modifications of HAp ceramics by changing the surface wettability [9], [10], [74]. Such samples are more favourable for cell cultures because, due to improved surface wettability, osteoblastic adhesion and proliferation are also improved [9] and osteoclast resorption is promoted [75].

In this study, contact angle measurements of apatite coatings of various structures were performed (Fig. 3.22) before and after polarization in an electric field. It can be seen that for both oriented and randomly oriented HAp coatings and low-crystallinity CaP coatings, the initial contact angles are quite high, $69.6 \pm 1.6^\circ$, $84.4 \pm 0.6^\circ$, and $83.7 \pm 0.8^\circ$, respectively. Indicating the hydrophobicity of the coating, which significantly decreases to $28.2 \pm 1.8^\circ$, $30.2 \pm 2.3^\circ$ and $28.3 \pm 2.5^\circ$ after polarization in an electric field, becoming already much more hydrophilic coatings. Contact angles were measured on negatively charged surfaces.

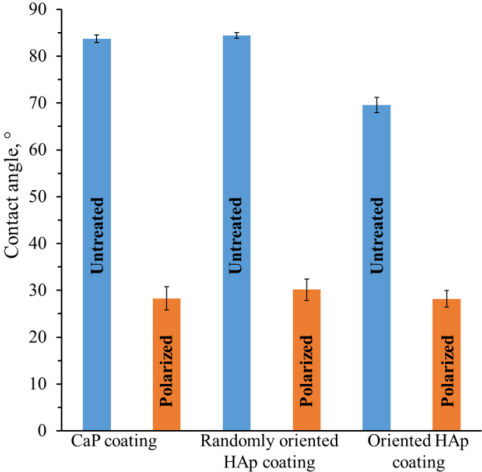


Fig. 3.22. Contact angle of apatite coatings with different structures in the as-sprayed state and after polarization.

Correlating the surface charge, wettability and surface energy of electrically polarized HAP has demonstrated the effect of these parameters on early-stage mineralization and bone cell interactions [37], [76], showing that contact angles decrease with increasing polarization temperature on both positively and negatively charged surfaces.

CONCLUSIONS

1. A surface charge can be imparted on amorphous calcium phosphate by electric polarization. The surface charge was $4.5 \mu\text{C}/\text{cm}^2$ on spark-plasma sintered carbonate-containing amorphous calcium phosphate pellets, compared to $8.1 \pm 2 \mu\text{C}/\text{cm}^2$ on thermally sprayed amorphous calcium phosphate coatings containing low content of crystalline phases.
2. An increase in the electric polarization temperature increases the charge on hydroxyapatite coatings with $\langle 001 \rangle$ crystal structure: an increase from $0.06 \mu\text{C}/\text{cm}^2$ to $2.6 \mu\text{C}/\text{cm}^2$ at temperatures from $300 \text{ }^\circ\text{C}$ to $450 \text{ }^\circ\text{C}$. A surface charge could not be measured for lower electric polarization temperatures.
3. For apatite, the highest surface charge ($10.9 \mu\text{C}/\text{cm}^2$) was recorded for the hydroxyapatite coating with randomly oriented crystals, while the lowest ($1.8 \pm 0.7 \mu\text{C}/\text{cm}^2$) was for the hydroxyapatite coating with $\langle 001 \rangle$ crystal orientation. The inclusion of hydroxyl ions in the oriented hydroxyapatite did not increase the stored charge.
4. The contact angles can be lowered by electrically polarizing calcium phosphate coatings. The contact angle decreased significantly (even by $\sim 66 \%$ for coating with randomly oriented crystals) after polarization, thereby improving the surface wettability.
5. The possibility to determine the hydroxyl ion content in the thermally-sprayed crystallized amorphous phase was partially confirmed. The as-sprayed amorphous calcium phosphate contained a low crystalline content, that after heating in vacuum formed calcium phosphate phases with an absence of hydroxyl ions (a mixture of tetracalcium phosphate, oxyapatite and α -tricalcium phosphate) and hydroxyapatite indicating the presence of hydroxyl ions. The loss of hydroxyl ions during heating in vacuum over time indicated easier release of hydroxyl ions in an amorphous phase and provided the basis for determining the kinetics of hydroxyl ion release.

References

- [1] J. Kobi Stern, E. E. Hahn, C. I. Evian, J. Waasdorp, E.S. Rosenberg, Implant failure: Prevalence, risk factors, management, and prevention, in: *Dent. Implant Complicat. Etiol. Prev. Treat. Second Ed.*, 2015: pp. 153–169. <https://doi.org/10.1002/9781119140474.ch8>.
- [2] S. Bohara, J. Suthakorn, Surface coating of orthopedic implant to enhance the osseointegration and reduction of bacterial colonization: a review, *Biomater. Res.* 26 (2022) 1–17. <https://doi.org/10.1186/s40824-022-00269-3>.
- [3] J. C. Elliott, Structure and Chemistry of the Apatites and Other Calcium Orthophosphates, *Stud. Inorg. Chem. Volume 18* (1994) 404. <https://doi.org/http://dx.doi.org/10.1016/B978-0-444-81582-8.50001-8>.
- [4] R. B. Borgens, Endogenous ionic currents traverse intact and damaged bone, *Science* (80-.). 225 (1984) 478–482. <https://doi.org/10.1126/science.6740320>.
- [5] C. Andrew, L. Bassett, R. O. Becker, Generation of electric potentials by bone in response to mechanical stress, *Science* (80-.). 137 (1962) 1063–1064.
- [6] B. Reid, M. Zhao, The Electrical Response to Injury: Molecular Mechanisms and Wound Healing, *Adv. Wound Care.* 3 (2014) 184–201. <https://doi.org/10.1089/wound.2013.0442>.
- [7] B. M. Isaacson, R. D. Bloebaum, Bone bioelectricity: What have we learned in the past 160 years?, *J. Biomed. Mater. Res. - Part A.* 95 (2010) 1270–1279. <https://doi.org/10.1002/jbm.a.32905>.
- [8] K. Yamashita, N. Oikawa, T. Umegaki, Acceleration and deceleration of bone-like crystal growth on ceramic hydroxyapatite by electric poling, *Chem. Mater.* 8 (1996) 2697–2700. <https://doi.org/10.1021/cm9602858>.
- [9] M. Nakamura, A. Nagai, T. Hentunen, J. Salonen, Y. Sekijima, T. Okura, K. Hashimoto, Y. Toda, H. Monma, K. Yamashita, Surface electric fields increase osteoblast adhesion through improved wettability on hydroxyapatite electrode, *ACS Appl. Mater. Interfaces.* 1 (2009) 2181–2189. <https://doi.org/10.1021/am900341v>.
- [10] S. Bodhak, S. Bose, A. Bandyopadhyay, Role of surface charge and wettability on early stage mineralization and bone cell-materials interactions of polarized hydroxyapatite, *Acta Biomater.* 5 (2009) 2178–2188. <https://doi.org/10.1016/j.actbio.2009.02.023>.
- [11] M. Nakamura, A. Nagai, Y. Tanaka, Y. Sekijima, K. Yamashita, Polarized hydroxyapatite promotes spread and motility of osteoblastic cells, *J. Biomed. Mater. Res. - Part A.* 92 (2010) 783–790. <https://doi.org/10.1002/jbm.a.32404>.
- [12] S. Itoh, S. Nakamura, M. Nakamura, K. Shinomiya, K. Yamashita, Enhanced bone ingrowth into hydroxyapatite with interconnected pores by Electrical Polarization, *Biomaterials.* 27 (2006) 5572–5579. <https://doi.org/10.1016/j.biomaterials.2006.07.007>.
- [13] T. Kobayashi, S. Nakamura, K. Yamashita, Enhanced osteobonding by negative surface charges of electrically polarized hydroxyapatite, *J. Biomed. Mater. Res.* 57 (2001) 477–484. [https://doi.org/10.1002/1097-4636\(20011215\)57:4<477::AID-JBM1193>3.0.CO;2-5](https://doi.org/10.1002/1097-4636(20011215)57:4<477::AID-JBM1193>3.0.CO;2-5).
- [14] W. Wang, S. Itoh, Y. Tanaka, A. Nagai, K. Yamashita, Comparison of enhancement of bone ingrowth into hydroxyapatite ceramics with highly and poorly interconnected pores by electrical polarization, *Acta Biomater.* 5 (2009) 3132–3140. <https://doi.org/10.1016/j.actbio.2009.04.036>.
- [15] M. Shariful Islam, M. Abdulla-Al-Mamun, A. Khan, M. Todo, Excellency of Hydroxyapatite Composite Scaffolds for Bone Tissue Engineering, *Biomaterials.* 10 (2020) 1–22. <https://doi.org/10.5772/intechopen.92900>.
- [16] R. F. Vargas-Coronado, L. H. Chan-Chan, J. M. Cervantes-Uc, J. V. Cauich-Rodríguez,

- M. C. Piña Barba, Characterization of bone cements prepared with either hydroxyapatite, α -TCP or bovine bone, *Rev. Mex. Ing. Biomed.* 34 (2013) 89–96.
- [17] W. Xue, S. Tao, X. Liu, X. Bin Zheng, C. Ding, In vivo evaluation of plasma sprayed hydroxyapatite coatings having different crystallinity, *Biomaterials*. 25 (2004) 415–421. [https://doi.org/10.1016/S0142-9612\(03\)00545-3](https://doi.org/10.1016/S0142-9612(03)00545-3).
- [18] P. O. Kroon, M. A. R. Freeman, Hydroxyapatite coating of hip prosthesis. Effect on migration into the femur, *J. Bone Jt. Surg. – Ser. B.* 74 (1992) 518–522. <https://doi.org/10.1302/0301-620x.74b4.1320620>.
- [19] B. Basu, Natural Bone and Tooth: Structure and Properties, in: *Biomater. Musculoskelet. Regen. Concepts*, Springer Singapore, Singapore, 2017: pp. 45–85. https://doi.org/10.1007/978-981-10-3059-8_3.
- [20] F. Betts, A.S. Posner, An x-ray radial distribution study of amorphous calcium phosphate, *Mater. Res. Bull.* 9 (1974) 353–360. [https://doi.org/10.1016/0025-5408\(74\)90087-7](https://doi.org/10.1016/0025-5408(74)90087-7).
- [21] J. D. Termine, A. S. Posner, Amorphous/crystalline interrelationships in bone mineral, *Calcif. Tissue Res.* 1 (1967) 8–23. <https://doi.org/10.1007/BF02008070>.
- [22] A. S. Posner, F. Betts, Synthetic amorphous calcium phosphate and its relation to bone mineral structure, *Bone Miner. Struct.* 8 (1975) 273–281.
- [23] K. Kaviyarasu, A. Mariappan, K. Neyvasagam, A. Ayeshamariam, P. Pandi, R. R. Palanichamy, C. Gopinathan, G. T. Mola, M. Maaza, Photocatalytic performance and antimicrobial activities of HAP-TiO₂ nanocomposite thin films by sol-gel method, *Surfaces and Interfaces*. 6 (2017) 247–255. <https://doi.org/10.1016/j.surfin.2016.10.002>.
- [24] R. B. Heimann, H. D. Lehmann, Technology of Coating Deposition, *Bioceram. Coatings Med. Implant.* (2015) 113–252. <https://doi.org/10.1002/9783527682294.ch5>.
- [25] K. A. Gross, C. C. Berndt, H. Herman, Amorphous phase formation in plasma-sprayed hydroxyapatite coatings, *J. Biomed. Mater. Res.* 39 (1998) 407–414. [https://doi.org/10.1002/\(SICI\)1097-4636\(19980305\)39:3<407::AID-JBM9>3.0.CO;2-N](https://doi.org/10.1002/(SICI)1097-4636(19980305)39:3<407::AID-JBM9>3.0.CO;2-N).
- [26] C. J. Liao, F. H. Lin, K. S. Chen, J. S. Sun, Thermal decomposition and reconstitution of hydroxyapatite in air atmosphere, *Biomaterials*. 20 (1999) 1807–1813. [https://doi.org/10.1016/S0142-9612\(99\)00076-9](https://doi.org/10.1016/S0142-9612(99)00076-9).
- [27] Y. Cao, J. Weng, J. Chen, J. Feng, Z. Yang, X. Zhang, Water vapour-treated hydroxyapatite coatings after plasma spraying and their characteristics, *Biomaterials*. 17 (1996) 419–424. [https://doi.org/10.1016/0142-9612\(96\)89658-X](https://doi.org/10.1016/0142-9612(96)89658-X).
- [28] R. Narayanan, S. K. Seshadri, T. Y. Kwon, K. H. Kim, Calcium phosphate-based coatings on titanium and its alloys, *J. Biomed. Mater. Res. — Part B Appl. Biomater.* 85 (2008) 279–299. <https://doi.org/10.1002/jbm.b.30932>.
- [29] D. He, X. Zhang, P. Liu, X. Liu, X. Chen, F. Ma, W. Li, K. Zhang, H. Zhou, Effect of hydrothermal treatment temperature on the hydroxyapatite coatings deposited by electrochemical method, *Surf. Coatings Technol.* 406 (2021) 126656. <https://doi.org/10.1016/j.surfcoat.2020.126656>.
- [30] R. Rodriguez, D. Rangel, G. Fonseca, M. Gonzalez, S. Vargas, Piezoelectric properties of synthetic hydroxyapatite-based organic-inorganic hydrated materials, *Results Phys.* 6 (2016) 925–932. <https://doi.org/10.1016/j.rinp.2016.11.005>.
- [31] N. Horiuchi, S. Nakaguki, N. Wada, K. Nozaki, M. Nakamura, A. Nagai, K. Katayama, K. Yamashita, Polarization-induced surface charges in hydroxyapatite ceramics, *J. Appl. Phys.* 116 (2014) 104902. <https://doi.org/10.1063/1.4886235>.
- [32] Y. Tanaka, T. Iwasaki, M. Nakamura, A. Nagai, K. Katayama, K. Yamashita, Polarization and microstructural effects of ceramic hydroxyapatite electrets, *J. Appl. Phys.* 107 (2010) 014107. <https://doi.org/10.1063/1.3265429>.

- [33] M. P. F. Graça, P. R. Prezas, The measurement of thermally stimulated depolarization and polarization currents, *NATO Sci. Peace Secur. Ser. B Phys. Biophys.* (2018) 121–137. https://doi.org/10.1007/978-94-024-1298-7_14.
- [34] N. Horiuchi, M. Nakamura, A. Nagai, K. Katayama, K. Yamashita, Proton conduction related electrical dipole and space charge polarization in hydroxyapatite, *J. Appl. Phys.* 112 (2012) 074901. <https://doi.org/10.1063/1.4754298>.
- [35] C. Combes, C. Rey, Amorphous calcium phosphates: Synthesis, properties and uses in biomaterials, *Acta Biomater.* 6 (2010) 3362–3378. <https://doi.org/10.1016/j.actbio.2010.02.017>.
- [36] P. R. Prezas, B. M. G. Melo, L. C. Costa, M. A. Valente, M. C. Lança, J. M. G. Ventura, L. F. V. Pinto, M. P. F. Graça, TSDC and impedance spectroscopy measurements on hydroxyapatite, β -tricalcium phosphate and hydroxyapatite/ β -tricalcium phosphate biphasic bioceramics, *Appl. Surf. Sci.* 424 (2017) 28–38. <https://doi.org/10.1016/j.apsusc.2017.02.225>.
- [37] S. Bodhak, S. Bose, A. Bandyopadhyay, Role of surface charge and wettability on early stage mineralization and bone cell-materials interactions of polarized hydroxyapatite, *Acta Biomater.* 5 (2009) 2178–2188. <https://doi.org/10.1016/j.actbio.2009.02.023>.
- [38] C. Rey, C. Combes, C. Drouet, D. Grossin, Bioactive ceramics: Physical chemistry, Elsevier Ltd., 2011. <https://doi.org/10.1016/b978-0-08-055294-1.00178-1>.
- [39] H. Li, B. S. Ng, K. A. Khor, P. Cheang, T. W. Clyne, Raman spectroscopy determination of phases within thermal sprayed hydroxyapatite splats and subsequent in vitro dissolution examination, *Acta Mater.* 52 (2004) 445–453. <https://doi.org/10.1016/j.actamat.2003.09.046>.
- [40] D. Grossin, S. Rollin-Martinet, C. Estournès, F. Rossignol, E. Champion, C. Combes, C. Rey, C. Geoffroy, C. Drouet, Biomimetic apatite sintered at very low temperature by spark plasma sintering: Physico-chemistry and microstructure aspects, *Acta Biomater.* 6 (2010) 577–585. <https://doi.org/10.1016/j.actbio.2009.08.021>.
- [41] J. Wen, Y. Leng, J. Chen, C. Zhang, Chemical gradient in plasma-sprayed HA coatings, *Biomaterials.* 21 (2000) 1339–1343. [https://doi.org/10.1016/S0142-9612\(99\)00273-2](https://doi.org/10.1016/S0142-9612(99)00273-2).
- [42] C. Combes, C. Rey, Amorphous calcium phosphates: Synthesis, properties and uses in biomaterials, *Acta Biomater.* 6 (2010) 3362–3378. <https://doi.org/10.1016/j.actbio.2010.02.017>.
- [43] N. Vandecandelaere, C. Rey, C. Drouet, Biomimetic apatite-based biomaterials: On the critical impact of synthesis and post-synthesis parameters, *J. Mater. Sci. Mater. Med.* 23 (2012) 2593–2606. <https://doi.org/10.1007/s10856-012-4719-y>.
- [44] C. Drouet, F. Bosc, M. Banu, C. Largeot, C. Combes, G. Dechambre, C. Estournès, G. Raimbeaux, C. Rey, Nanocrystalline apatites: From powders to biomaterials, *Powder Technol.* 190 (2009) 118–122. <https://doi.org/10.1016/j.powtec.2008.04.041>.
- [45] N. Doebelin, R. Kleeberg, Profex: A graphical user interface for the Rietveld refinement program BGMN, *J. Appl. Crystallogr.* 48 (2015) 1573–1580. <https://doi.org/10.1107/S1600576715014685>.
- [46] M. Inagaki, T. Kameyama, Phase transformation of plasma-sprayed hydroxyapatite coating with preferred crystalline orientation, *Biomaterials.* 28 (2007) 2923–2931. <https://doi.org/10.1016/j.biomaterials.2007.03.008>.
- [47] K. A. Gross, C. C. Berndt, Thermal processing of hydroxyapatite for coating production, *J. Biomed. Mater. Res.* 39 (1998) 580–587. [https://doi.org/10.1002/\(SICI\)1097-4636\(19980315\)39:4<580::AID-JBM12>3.0.CO;2-B](https://doi.org/10.1002/(SICI)1097-4636(19980315)39:4<580::AID-JBM12>3.0.CO;2-B).
- [48] L. Sun, C. C. Berndt, C. P. Grey, Phase, structural and microstructural investigations of plasma sprayed hydroxyapatite coatings, *Mater. Sci. Eng. A.* 360 (2003) 70–84. [https://doi.org/10.1016/S0921-5093\(03\)00439-8](https://doi.org/10.1016/S0921-5093(03)00439-8).

- [49] S. Koutsopoulos, Synthesis and characterization of hydroxyapatite crystals: A review study on the analytical methods, *J. Biomed. Mater. Res.* 62 (2002) 31–34. <https://doi.org/10.1002/jbm.10280>.
- [50] C. Ortali, I. Julien, C. Drouet, E. Champion, Influence of carbonation on the low-temperature consolidation by Spark Plasma Sintering of carbonated calcium phosphate bioceramics, *Ceram. Int.* 46 (2020) 5799–5810. <https://doi.org/10.1016/j.ceramint.2019.11.030>.
- [51] I. Demnati, D. Grossin, C. Combes, C. Rey, Plasma-Sprayed apatite Coatings: Review of physical-chemical characteristics and their biological consequences, *J. Med. Biol. Eng.* 34 (2014) 1–7. <https://doi.org/10.5405/jmbe.1459>.
- [52] L. Pluduma, Hydroxyl Ion Quantification in Hydroxyapatite and the Effect on the biological response, Riga Technical University, 2017.
- [53] A. Kafilak, W. Kolodziejski, Complementary information on water and hydroxyl groups in nanocrystalline carbonated hydroxyapatites from TGA, NMR and IR measurements, *J. Mol. Struct.* 990 (2011) 263–270. <https://doi.org/10.1016/j.molstruc.2011.01.056>.
- [54] M. Ashok, S. N. Kalkura, N. M. Sundaram, D. Arivuoli, Growth and characterization of hydroxyapatite crystals by hydrothermal method, *J. Mater. Sci. Mater. Med.* 18 (2007) 895–898. <https://doi.org/10.1007/s10856-006-0070-5>.
- [55] W. Chen, T. Long, Y. J. Guo, Z. A. Zhu, Y. P. Guo, Hydrothermal synthesis of hydroxyapatite coatings with oriented nanorod arrays, *RSC Adv.* 4 (2014) 185–191. <https://doi.org/10.1039/c3ra43664k>.
- [56] R. B. Heimann, Thermal spraying of biomaterials, *Surf. Coatings Technol.* 201 (2006) 2012–2019. <https://doi.org/10.1016/j.surfcoat.2006.04.052>.
- [57] L. Pluduma, K. A. Gross, C. Rey, A. Ubelis, A. Berzina, Production and characterization of oxyhydroxyapatites, *Key Eng. Mater.* 762 (2018) 48–53. <https://doi.org/10.4028/www.scientific.net/KEM.762.48>.
- [58] C. Rey, C. Combes, C. Drouet, A. Lebugle, H. Sfihi, A. Barroug, Nanocrystalline apatites in biological systems: Characterisation, structure and properties, *Materwiss. Werksttech.* 38 (2007) 996–1002. <https://doi.org/10.1002/mawe.200700229>.
- [59] C. Rey, O. Marsan, C. Combes, C. Drouet, D. Grossin, S. Sarda, Characterization of Calcium Phosphates Using Vibrational Spectroscopies, in: *Adv. Calcium Phosphate Biomater.*, 2014: pp. 229–266. <https://doi.org/10.1007/978-3-642-53980-0>.
- [60] N. Horiuchi, J. Endo, N. Wada, K. Nozaki, M. Nakamura, A. Nagai, K. Katayama, K. Yamashita, Dielectric properties of stoichiometric and defect-induced hydroxyapatite, *J. Appl. Phys.* 113 (2013) 134905. <https://doi.org/10.1063/1.4799130>.
- [61] S. Nakamura, H. Takeda, K. Yamashita, Proton transport polarization and depolarization of hydroxyapatite ceramics, *J. Appl. Phys.* 89 (2001) 5386–5392. <https://doi.org/10.1063/1.1357783>.
- [62] M. Shahrooz Amin, T. F. Peterson, M. Zahn, Measurements of electric charge associated with evaporation and condensation of water on metallic surfaces as a consequence of pressure, humidity, and temperature change, *J. Electrostat.* 64 (2006) 597–603. <https://doi.org/10.1016/j.elstat.2005.10.014>.
- [63] C. Ortali, I. Julien, C. Drouet, E. Champion, Influence of carbonation on the low-temperature consolidation by Spark Plasma Sintering of carbonated calcium phosphate bioceramics, *Ceram. Int.* (2019). <https://doi.org/10.1016/j.ceramint.2019.11.030>.
- [64] M. Luginina, R. Orru, G. Cao, M. Luginina, D. Grossin, F. Brouillet, G. Chevallier, C. Thouron, C. Drouet, First successful stabilization of consolidated amorphous calcium phosphate (ACP) by cold sintering: Toward highly-resorbable reactive bioceramics, *J. Mater. Chem. B.* 8 (2020) 629–635. <https://doi.org/10.1039/c9tb02121c>.
- [65] A. A. Joksa, L. Komarovska, D. Ubele-Kalnina, A. Viksna, K. A. Gross, Role of

- carbonate on the crystallization and processing of amorphous calcium phosphates, *Materialia*. 27 (2023) 101672. <https://doi.org/10.1016/j.mtla.2022.101672>.
- [66] C. Rey, B. Collins, T. Goehl, I. R. Dickson, M.J. Glimcher, The carbonate environment in bone mineral: A resolution-enhanced fourier transform infrared spectroscopy study, *Calcif. Tissue Int.* 45 (1989) 157–164. <https://doi.org/10.1007/BF02556059>.
- [67] K. Yamashita, K. Kitagaki, T. Umegaki, Thermal Instability and Proton Conductivity of Ceramic Hydroxyapatite at High Temperatures, *J. Am. Ceram. Soc.* 78 (1995) 1191–1197. <https://doi.org/10.1111/j.1151-2916.1995.tb08468.x>.
- [68] M. Ueshima, S. Nakamura, K. Yamashita, Huge, Millicoulomb Charge Storage in Ceramic Hydroxyapatite by Bimodal Electric Polarization, *Adv. Mater.* 14 (2002) 591. [https://doi.org/10.1002/1521-4095\(20020418\)14:8<591::aid-adma591>3.0.co;2-7](https://doi.org/10.1002/1521-4095(20020418)14:8<591::aid-adma591>3.0.co;2-7).
- [69] N. Horiuchi, K. Madokoro, K. Nozaki, M. Nakamura, K. Katayama, A. Nagai, K. Yamashita, Electrical conductivity of polycrystalline hydroxyapatite and its application to electret formation, *Solid State Ionics*. 315 (2018) 19–25. <https://doi.org/10.1016/j.ssi.2017.11.029>.
- [70] K. Tanaka, S. Nakamura, K. Yoshida, K. Hashimoto, Y. Toda, K. Yamashita, Effects of Electrical Polarization on B-Type Carbonated Hydroxyapatite, *Phosphorus Res. Bull.* 17 (2004) 126–129. https://doi.org/10.3363/prb1992.17.0_126.
- [71] A. Nagai, K. Tanaka, Y. Tanaka, M. Nakamura, K. Hashimoto, K. Yamashita, Electric polarization and mechanism of B-type carbonated apatite ceramics, *J. Biomed. Mater. Res. – Part A*. 99 A (2011) 116–124. <https://doi.org/10.1002/jbm.a.33131>.
- [72] K. A. Gross, D. Muller, H. Lucas, D. R. Haynes, Osteoclast resorption of thermal spray hydroxyapatite coatings is influenced by surface topography, *Acta Biomater.* 8 (2012) 1948–1956. <https://doi.org/10.1016/j.actbio.2012.01.023>.
- [73] K. A. Gross, C. Petzold, L. Pluduma-Lafarge, M. Kumermanis, H. J. Haugen, Structural and chemical hierarchy in hydroxyapatite coatings, *Materials (Basel)*. 13 (2020) 4447. <https://doi.org/10.3390/ma13194447>.
- [74] M. Nakamura, N. Hori, S. Namba, T. Toyama, N. Nishimiya, K. Yamashita, Wettability and surface free energy of polarised ceramic biomaterials, *Biomed. Mater.* 10 (2015) 11001. <https://doi.org/10.1088/1748-6041/10/1/011001>.
- [75] L. Bergara-Muguruza, K. Mäkelä, T. Yrjälä, J. Salonen, K. Yamashita, M. Nakamura, Surface Electric Fields Increase Human Osteoclast Resorption through Improved Wettability on Carbonate-Incorporated Apatite, *ACS Appl. Mater. Interfaces*. 13 (2021) 58270–58278. <https://doi.org/10.1021/acsami.1c14358>.
- [76] M. Nakamura, N. Hori, H. Ando, S. Namba, T. Toyama, N. Nishimiya, K. Yamashita, Surface free energy predominates in cell adhesion to hydroxyapatite through wettability, *Mater. Sci. Eng. C*. 62 (2016) 283–292. <https://doi.org/10.1016/j.msec.2016.01.037>.



Dārta Ūbele-Kalniņa was born in 1990 in Riga. She obtained a Bachelor's degree (2012) and a Master's degree in Chemistry (2014) from the University of Latvia. She has worked at the Institute of Atomic Physics and Spectroscopy of the University of Latvia and the Latvian State Institute of Wood Chemistry. Since 2016, she has been with the Faculty of Materials Science and Applied Chemistry of Riga Technical University, initially as a research assistant, but since 2018, as a researcher. She is currently a researcher at the Institute of Materials and Surface Engineering of RTU. Her scientific interests are related to the production of calcium phosphate bioceramics, their surface modifications in an electric field, and quantitative determination of hydroxyl ions by FTIR spectrometry using the deconvolution model.